doi:10.1093/brain/awx056 BRAIN 2017: 140; 1399–1419 | 1399

BRAIN
A JOURNAL OF NEUROLOGY

Glycation potentiates α-synuclein-associated neurodegeneration in synucleinopathies

Hugo Vicente Miranda,[1,2] Éva M. Szegő,[3] Luís M. A. Oliveira,[4,5] Carlo Breda,[6] Ekrem Darendelioglu,[6,7] Rita M. de Oliveira,[1,2] Diana G. Ferreira,[2,3] Marcos A. Gomes,[2] Ruth Rott,[8] Márcia Oliveira,[2] Francesca Munari,[9,10] Francisco J. Enguita,[2] Tânia Simões,[11] Eva F. Rodrigues,[3] Michael Heinrich,[12] Ivo C. Martins,[2] Irina Zamolo,[13] Olaf Riess,[13] Carlos Cordeiro,[14] Ana Ponces-Freire,[14] Hilal A. Lashuel,[15] Nuno C. Santos,[2] Luisa V. Lopes,[2] Wei Xiang,[16] Thomas M. Jovin,[5] Deborah Penque,[11] Simone Engelender,[8] Markus Zweckstetter,[9,10,17] Jochen Klucken,[12] Flaviano Giorgini,[6] Alexandre Quintas[4] and Tiago F. Outeiro[1,3,18]

α-Synuclein misfolding and aggregation is a hallmark in Parkinson's disease and in several other neurodegenerative diseases known as synucleinopathies. The toxic properties of α-synuclein are conserved from yeast to man, but the precise underpinnings of the cellular pathologies associated are still elusive, complicating the development of effective therapeutic strategies. Combining molecular genetics with target-based approaches, we established that glycation, an unavoidable age-associated post-translational modification, enhanced α-synuclein toxicity *in vitro* and *in vivo*, in *Drosophila* and in mice. Glycation affected primarily the N-terminal region of α-synuclein, reducing membrane binding, impaired the clearance of α-synuclein, and promoted the accumulation of toxic oligomers that impaired neuronal synaptic transmission. Strikingly, using glycation inhibitors, we demonstrated that normal clearance of α-synuclein was re-established, aggregation was reduced, and motor phenotypes in *Drosophila* were alleviated. Altogether, our study demonstrates glycation constitutes a novel drug target that can be explored in synucleinopathies as well as in other neurodegenerative conditions.

1 CEDOC, Chronic Diseases Research Centre, NOVA Medical School | Faculdade de Ciências Médicas, Universidade NOVA de Lisboa, Campo dos Mártires da Pátria, 130, 1169-056 Lisboa, Portugal
2 Instituto de Medicina Molecular, Faculdade de Medicina, Universidade de Lisboa, Lisboa, Portugal
3 Department of Neurodegeneration and Restorative Research, Center for Nanoscale Microscopy and Molecular Physiology of the Brain (CNMPB), Center for Biostructural Imaging of Neurodegeneration (BIN), University Medical Center Göttingen, Waldweg 33, 37073 Göttingen, Germany
4 Centro de Investigação Interdisciplinar Egas Moniz, Instituto Superior de Ciências da Saúde Egas Moniz, 2829-511 Monte de Caparica, Caparica, Portugal
5 Laboratory of Cellular Dynamics, Max Planck Institute for Biophysical Chemistry, 37077 Göttingen, Germany
6 Department of Genetics, University of Leicester, Leicester LE1 7RH, UK
7 Bingol University, Science and Letters Faculty, Molecular Biology and Genetics Department, 12000, Bingol, Turkey
8 Department of Biochemistry, Rappaport Faculty of Medicine and Research Institute, Technion-Israel Institute of Technology, Haifa 31096, Israel
9 Department for NMR-based Structural Biology, Max Planck Institute for Biophysical Chemistry, 37077 Göttingen, Germany
10 German Center for Neurodegenerative Diseases (DZNE), 37077 Göttingen, Germany
11 Laboratório de Proteómica, Departamento de Genética Humana, Instituto Nacional de Saúde Dr. Ricardo Jorge, 1649-016 Lisboa, Portugal
12 Department of Molecular Neurology, University Hospital Erlangen, Schwabachanlage 6, 91054 Erlangen, Germany
13 Institute of Medical Genetics and Applied Genomics, University of Tuebingen, 72074 Tuebingen, Germany

Received June 29, 2016. Revised January 17, 2017. Accepted January 20, 2017. Advance Access publication April 10, 2017.

14 Enzymology Group, Departamento de Quimica e Bioquimica, Centro de Quimica e Bioquimica, Faculdade de Ciencias da Universidade de Lisboa, Campo Grande, Edificio C8, 1749-016, Lisboa, Portugal
15 Laboratory of Molecular and Chemical Biology of Neurodegeneration, Swiss Federal Institute of Technology Lausanne (EPFL), FSV-BMI AI 2137.1, Station 15, CH-1015 Lausanne, Switzerland
16 Institute for Biochemistry, Friedrich-Alexander-University Erlangen-Nürnberg (FAU), Erlangen, Germany
17 Center for Nanoscale Microscopy and Molecular Physiology of the Brain, University Medical Center, 37075 Göttingen, Germany
18 Max Plank Institute for Experimental Medicine, Goettingen, Germany

Correspondence to: Tiago Fleming Outeiro
Department of Neurodegeneration and Restorative Research, Center for Nanoscale Microscopy and Molecular Physiology of the Brain (CNMPB), University Medical Center Göttingen, Waldweg 33, 37073 Göttingen, Germany
E-mail: touteir@gwdg.de

Keywords: glycation; Parkinson's disease; neurodegeneration; alpha-synuclein

Abbreviations: AGEs = advanced glycation end-products; CEL = *N*(epsilon)-(carboxyethyl)lysine; fEPSP = evoked field synaptic potential; iPSC = induced pluripotent stem cell; LTP = long term potentiation; LUHMES = Lund human mesencephalic cells; MGO = methylglyoxal; SUV = small unilamellar vesicle

Introduction

The molecular underpinnings of neurodegenerative diseases such as Parkinson's disease and Alzheimer's disease remain unclear, as genetics explains only a minor fraction of cases. Therefore, the study of non-genetic factors that may contribute to the development of neurodegenerative diseases is urgent. Neurodegenerative diseases are known to be associated with the misfolding and accumulation of various proteins. Parkinson's disease is a common disorder known for typical motor features that result from the loss of nigrostriatal dopaminergic neurons (DA), and for the accumulation of pathognomonic intraneuronal inclusions known as Lewy bodies and Lewy neurites. These inclusions are primarily composed of α-synuclein (Spillantini *et al.*, 1998; Wales *et al.*, 2013), a protein also associated with other disorders known as synucleinopathies.

We and others have extensively exploited yeast cells expressing neurodegenerative disease-associated proteins to recapitulate important cellular pathologies, thereby accelerating our understanding of the molecular basis of these disorders (Outeiro and Lindquist, 2003; Tenreiro and Outeiro, 2010). Recently, we found that DJ-1, the product of the *PARK7* gene, interacts with and protects against α-synuclein aggregation and toxicity in yeast and in mammalian cell models of Parkinson's disease (Zondler *et al.*, 2014). DJ-1 mutations cause autosomal recessive Parkinson's disease through a loss-of-function mechanism. Recently, this protein was shown to have both glyoxalase (Lee *et al.*, 2012) and deglycase activities (Richarme *et al.*, 2015), suggesting glycation, an unavoidable age-associated process, might play a role in Parkinson's disease. In a previous unbiased genetic screen in yeast, we identified another component of the glyoxalase system (Glo4) as an enhancer of α-synuclein toxicity (Willingham *et al.*, 2003). In fact, glucose is readily metabolized generating reducing sugars that covalently react with proteins generating advanced glycation end-products (AGEs) that invariably impact on protein function (Vicente Miranda and Outeiro, 2010). Intriguingly, diabetes, a widespread condition of impaired glucose metabolism, has been established as an important risk factor for Parkinson's disease (Hu *et al.*, 2007; Sun *et al.*, 2012; Vicente Miranda *et al.*, 2016*a*). The levels of AGEs are increased in the brains of patients suffering from synucleinopathy (Dalfo *et al.*, 2005), and AGEs can be detected at the periphery of Lewy bodies (Castellani *et al.*, 1996). A similar staining pattern of AGEs was reported in early Lewy bodies in patients with Lewy body disease. This suggested that an excess of carbonyl compounds could play a role in the pathogenesis of Parkinson's disease (Munch *et al.*, 2000). However, it has been unclear whether AGEs are causally related to disease and whether α-synuclein is glycated. Here, we asked whether manipulation of the major component of the glyoxalase system (GLO1) would affect α-synuclein aggregation and toxicity. GLO1 constitutes a major line of defence against methylglyoxal (MGO), a dicarbonyl metabolite that is formed unavoidably via multiple catabolic processes (Reichard *et al.*, 1986; Lyles and Chalmers, 1992; Richard, 1993; Thornalley *et al.*, 1999; Baynes and Thorpe, 2000). MGO glycates arginine and lysine residues. With the latter, MGO forms *N*(epsilon)-(carboxyethyl)lysine (CEL) (Ahmed *et al.*, 1997) and the imidazolium crosslink, methylglyoxal-lysine dimer (MOLD) (Frye *et al.*, 1998). Glo1 activity depends on reduced forms of glutathione (GSH), to which MGO reversibly associates with, forming an MGO-GSH hemithioacetal (substrate of GLO1), and NADPH, respectively (Vander Jagt *et al.*, 1992; Gomes *et al.*, 2005). Therefore, the catabolism of MGO leads to a decrease in the levels of these cofactors, which are also crucial for oxidative stress responses. Interestingly, in hyperglycaemia conditions and in diabetic patients, MGO is increased, leading to higher MGO-glycation levels (2–4-fold) (Yao and Brownlee, 2010; Bierhaus *et al.*, 2012). Notably, the brain's defences against glycation, such as GSH and GLO1, decrease with ageing (Chen *et al.*, 1989; Kuhla *et al.*, 2006), and in the substantia nigra of Parkinson's disease patients (Pearce *et al.*, 1997), suggesting that MGO levels may increase with

ageing and in Parkinson's disease. Altogether, determining the molecular mechanisms through which glycation alters proteostasis and contributes to synucleinopathies enables an important breakthrough that links ageing to neurodegeneration and uncovers novel therapeutic targets for intervention in synucleinopathies.

Materials and methods

MGO purification

MGO was produced as in Gomes *et al.* (2005). Briefly, MGO was prepared by sulphuric acid hydrolysis of 1,1-dimethyl acetal. The resulting MGO was purified by fractional distillation under reduced pressure and nitrogen bleed. MGO was evaporated at ~72°C and three fractions were obtained. The first fraction was discarded, as it contained MGO mixed with methanol. The second fraction was collected and stored at −80°C until further use.

α-Synuclein aggregation and toxicity in yeast

Saccharomyces cerevisiae strain BY4741 and mutant strains Δ*glo1* and Δ*tpi* (Euroscarf collection) were used. Cells were grown and transformed as in Vicente Miranda *et al.* (2013). Briefly, α-synuclein and familial variants A30P, E46K and A53T were expressed using the p426 GPD vector after transformation into yeast cells using the lithium acetate method. Transformants were selected in Yeast Nitrogen Base complete media without uracil (YNB-U). D-Glucose treatment was performed challenging cells for 24 h with 4% D-glucose in media. Fluorescent micrographs were acquired with a Zeiss Axiovert 200M. Toxicity assays were performed as previously (Outeiro and Lindquist, 2003) by spotting serial dilutions of yeast cells onto agar-YNB-U plates. Cell viability was assessed by counting colony-forming units (CFUs) after growth for 2 days at 30°C on YEP-glucose as previously described (Tenreiro *et al.*, 2014*b*).

H4 cells immunocytochemistry, immunoblotting and toxicity

H4 neuroglioma cells were maintained, grown and transfected with α-synuclein, an aggregation-prone variant of α-synuclein (SynT) and synphilin-1 (Synph 1) as in Vicente Miranda *et al.* (2013) with FuGENE® 6 (Roche) using standard procedures. Twenty-four hours after SynT and Synph 1 co-transfection, cells seeded at 20 000 cells/cm^2 in 35 mm imaging dishes (Ibidi) or seeded at 30 000 cells/cm^2 in 10 cm, 6 cm, 6-well plates or 12-well plates (TPP) were treated with vehicle (H_2O) or MGO (0.5 mM) for 16 h. Cells washed with phosphate-buffered saline (PBS) were fixed and permeabilized in 100% ice-cold methanol (−20°C, 10 min). Cells were incubated with blocking solution (1.5% normal goat serum in PBS) for 1 h at room temperature. Cells were incubated with the primary antibody anti-α-synuclein (Cell Signaling Technology, 2642) 1:75 in blocking solution, overnight at 4°C alone, or co-stained with anti-ubiquitin antibody (Abcam, P4G7) 1:500 in blocking solution. Cells, washed with PBS, were incubated for 4 h at room temperature with Alexa Fluor® 488 goat anti-rabbit conjugated secondary antibody (Invitrogen, A11008) or Alexa Fluor® 568 goat anti-mouse conjugated secondary antibody (Invitrogen, A11031) using a dilution of 1:1000 in blocking solution. Widefield fluorescent microscope Zeiss Axiovert 200M (Carl Zeiss MicroImaging) and point scanning confocal microscope Zeiss LSM 710 were used to visualize α-synuclein inclusions.

Sucrose gradient fractions were applied in a dot-blot system and immunoblotting performed according to standard procedures (Basso *et al.*, 2013). For immunoblotting, we used the following antibodies: anti aSyn (BD Transduction laboratories, S63320, 1:3000); anti-V5 (Santa Cruz, SC-83849-R, 1:1000); anti-LC3 (Nano Tools, 0260-100/LC3-2G6, 1:2000); anti-β-actin (Ambion, AM4302, 1:5000); and anti-GAPDH (Ambion, AM4300, 1:5000).

Cytotoxicity was measured using Caspase-3 or lactate dehydrogenase (LDH) kit (Clontech). Total protein lysates were obtained as in Vicente Miranda *et al.* (2013).

α-Synuclein immunoprecipitation

H4 neuroglioma cells were transfected with α-synuclein or cotransfected with SynT and Synph 1. Twenty-four hours post-transfection, cells were challenged with PBS (Ctrl) or MGO (0.5 mM) for 16 h. Media was renewed and cells challenged for 6 h. Protein was extracted using immunoprecipitation (IP) buffer (150 mM Tris-HCl, pH 7.4, 1 mM EDTA, 1% NP-40, 0.1% SDS and complete protease inhibitors). Protein extract (500 mg) was precleared in 10 µl of protein G beaded agarose resin (Invitrogen) for 1 h under nutation at 4°C. Protein supernatant was incubated with 2.4 µg of anti α-synuclein antibody (BD Transduction laboratories, S63320) and nutated at 4°C overnight. Beads were collected and washed 4× in IP buffer. Samples were immunoblotted as previously indicated using anti-α-synuclein (C-20 Santa Cruz biotechnology, sc-7011-R, 1:1000) and anti-AGEs (Millipore, AB9890, 1:1000).

MGO measurement

MGO was extracted from yeast or H4 cells with $HClO_4$ 3 M at 4°C for 10 min and stored at −80°C. After derivatization with 1,2-phenylenediamine 0.92 mM and solid-phase extraction of quinoxalines, MGO levels (as 2-methylquinoxaline) were determined by reverse phase HPLC on a Merck Hitachi system: pump L-2130; column oven L-2300; UV detector L-2400. Samples were separated on LiChroCART LiChrospher® RP-18 endcapped (5 µm, 250–4.6) with methanol/ammonium formate 20 mM pH3.4 (60/40) used as mobile phase (1 ml/min); 20 µl as injection volume; and detection at 320 nm. Dimethylquinoxaline, added prior to solid-phase extraction was used as internal standard. MGO was normalized to dimethylquinoxaline.

LUHMES cells

Proliferating LUHMES (Lund human mesencephalic) cells (a kind gift of Prof. M. Leist, University of Konstanz, Germany) were cultivated in LUHMES proliferation medium

containing advanced DMEM/F12, 1% N2 supplement (Invitrogen), 2 mM L-glutamine (Gibco), and 40 ng/ml recombinant basic fibroblast growth factor (R&D Systems) on cell culture T75 and T175 flasks or multi-well plates (Nunc) precoated with 50 ng/ml poly-L-ornithine (PLO) and 1 µg/ml fibronectin (Sigma-Aldrich) at 37°C and 5% CO_2. Differentiated LUHMES cells were generated by replacing proliferation medium by differentiation medium containing advanced DMEM/F12, 1% N2 supplement, 2 mM L-glutamine, 1 mM dibutyryl 3′,5′-cyclic AMP, (Sigma-Aldrich), 1 µg/ml tetracycline, and 2 ng/ml recombinant human glial derived neurotrophic factor (R&D Systems). After 2 days, cells were seeded into PLO/fibronectin precoated multi-well plates.

Generation of stable expressing clonal LUHMES cells

Proliferating LUHMES cells were transduced by lentiviral delivery of α-synuclein-IRES-GFP (green fluorescent protein) or IRES-GFP constructs, a third-generation lentiviral system as described previously (Tiscornia *et al.*, 2006). Purified lentivirus encoding α-synuclein and GFP were kindly provided by Dr B. Winner (Interdisciplinary Center for Clinical Research, Nikolaus-Fiebiger Center for Molecular Medicine, Erlangen). Cloning of stably-expressing (GFP-positive) cells was performed by single cell colony culture using limited dilution (LUHMES cells).

MGO treatment of LUHMES cells

For MGO treatment, predifferentiated (Day 2) LUHMES cells were seeded into 96-well plates (0.75×10^5 cells) or into 24-well plates (0.3×10^6 cells) and incubated at 37°C, 5% CO_2 for 3 days. MGO stock was sterile filtered and prediluted 1:100 in sterile pure water. Predilution was again diluted in LUHMES differentiation medium. Cell culture medium was removed. MGO dilution (120 µl) was added at the indicated concentrations. Cells were then incubated at 37°C, 5% CO_2 until the measurement of toxicity.

LUHMES viability assay and immunocytochemistry

Cellular viability was determined by the conversion of (3-(4,5-dimethylthiazol-2-yl)-5-(3-carboxymethoxyphenyl)-2-(4-sulfophenyl)-2H-tetrazolium (MTS) to formazan, measured by the absorbance (490 nm) of intracellular formazan using a 96-well plate reader according to the manufacturer's protocol (MTS-assay, Promega).

For immunocytochemistry, cells were cultured on 13 mm glass coverslips in 24-well plates as described above. Cells were fixed for 15–20 min with 4% paraformaldehyde at room temperature, washed three times in Tris-phosphate-buffered solution (TBS) and incubated in fish skin gelatin buffer (FSGB) containing 0.1% Triton™ X-100 for 20 min at room temperature. Primary antibodies (rat anti-α-synuclein, 15G7, 1:250; rabbit anti-Caspase 3a, 1:500, Cell Signaling Technology) were diluted in FSGB and applied overnight at 4°C. After washing, secondary antibodies (dk-anti-rt, rhodamine, 1:500, Dianova; dk-anti-rb, diluted in 300 µl/well FSGB) were added and the plate was incubated at room temperature for 1 h in the dark. After removing the secondary antibody and washing once with FSGB, DAPI (diluted in 500 µl/well FSGB) was added and again incubated at room temperature for 15 min. The coverslips were mounted with ProLong® Antifade. Images were acquired using a Zeiss ApoTome microscope.

Differentiation of patient-derived induced pluripotent stem cells

The neuronal lineage control and patient human-induced pluripotent stem cells (iPSCs) were isolated and characterized by The Parkinson's Institute (Byers *et al.*, 2011; Mak *et al.*, 2012) and made available through a joint BMBF-CIRM grant to T.M.J. (315050 AZ0101). An extensive comparative characterization between control and *SNCA* triplication is presented in Oliveira *et al.* (2015). α-Synuclein knockdown (KD) in the triplication line was achieved with the transduction of a lentiviral shRNA using the pLKO.1 Puro vector containing the 5′ACCAAAGAGCAAGTGACAAAT-3′. Stage IV cells were cultivated and differentiated in two stages (Mak *et al.*, 2012): 10 days in DA1 medium (using 1 µM SAG) and 20 days in DA2 medium.

Cytotoxicity in induced pluripotent stem cells

Differentiated iPSCs were washed with 'oxidative stress medium' (same formula as DA2 medium, but with a B-27 supplement lacking antioxidants) (Life Technologies) and MGO was directly added to medium. Cells were incubated at 37°C for 18 h and cytotoxicity assessed by measuring the cell supernatant with the LDH cytotoxicity detection kit (Roche Applied Science). The samples were measured in triplicate on a PHERAstar FS plate reader (BMG Labtech).

Drosophila lines

Flies were raised at 25°C in LD12:12 on standard maize food. The *elav-GAL4* (c155), *w*;*UASeGFP*;+(5431) and *w*;+;*UAS-aSyn* (8146) transgenic lines were obtained from the Bloomington Stock Center (Bloomington, Indiana). RNAi transgenic lines were obtained from the Vienna *Drosophila* RNAi Center (VDRC). For *Glo1* knockdown, the 101560 line from the KK Library (phiC31-based transgenes at a single, defined site) was used. For *Tpi* knockdown, two lines were used from the GD Library (P-element based, random insertion site): 25643 (Fig. 2) and 25644 (Supplementary Fig. 3).

Negative geotaxis and survival assays

Negative geotaxis assays were performed as described (Ali *et al.*, 2011). The same fly groups were tested at Days 10, 20 and 30 post-eclosion. For the survival assay, female flies of the desired genotype were collected and kept in groups of 10 in separate vials. Flies were passaged onto fresh food every 2–3 days and the number of dead individuals was scored.

Glycation studies in mice

Animal experiments were performed according to institutional and national regulations.

Brains from 4- (young) and 22-month-old (old) mice expressing human α-synuclein, were quickly removed and homogenized in RIPA buffer in the presence of protease and phosphatase inhibitors (Roche Complete and PhosStop). Brains from 2.5- (young), 11- and 17-month-old (old) wild-type mice were also processed.

Old male mice (6–7 months old) expressing human α-synuclein under the control of the Thy-1 promoter (α-synuclein transgenic) (Rockenstein *et al.*, 2002) or B6D2F1 wild-type littermate controls received MGO, or vehicle (PBS, pH 7.4) injection under deep anaesthesia (80 mg/kg ketamine hydrochloride, 5 mg/kg xylasine hydrochloride). 2 × 1 µl of MGO (340 mM) or PBS were injected into the substantia nigra (stereotactic coordinates: AP: 3.1; L: −1.2; DV: −4.2 from Bregma) or the striatum (stereotactic coordinates: AP: 0.86; L: −1.5; DV: 5/5.5 from dura) using glass microcapillary with a flow rate of 250 nl/min.

For immunohistochemistry, mice were transcardially perfused with 4% paraformaldehyde (PFA) 7 days post-injection. Brains were removed and post-fixed for 2 h at 4°C and then cryoprotected in TBS (pH 7.6) containing 30% sucrose (w/v) overnight at 4°C. Coronal free-floating sections (30 µm) were stained as reported previously (Szego *et al.*, 2012). Briefly, sections were incubated either with anti-tyrosine hydroxylase (TH) rabbit (Millipore, 1:1000), anti-CEL (Cosmobio, 1:1000), anti-aSyn (610786, 1:1000, BD Transduction laboratories), anti-phospho-synuclein (Ser129) (pSyn, Wako, 1:1000), anti-vesicular monoamine transporter (VMAT, 1:2000, Abcam), anti-NeuN mouse (Millipore, 1:1000) or anti-α-synuclein aggregation clone 5G4 (MABN389, 1:1000, Millipore) for 48 h at 4°C. Sections were then treated either with Alexa Fluor®-conjugated secondary antibody (1:1000, Invitrogen) or with biotinylated anti-mouse (NeuN) or anti-rabbit (TH) IgG (Vector Laboratories, 1:200) followed by avidin–biotin–horseradish peroxidase (HRP) complex (Vector Standard Elite® Kit, 1:500). Peroxidase labelling was visualized by diaminobenzidine tetrahydrochloride (DAB). Omission of the primary antibody resulted in no staining.

Numbers of TH-, VMAT-, DAPI- or NeuN-positive neurons were counted and estimated by using the optical dissector (StereoInvestigator; MBF Bioscience) (Szego *et al.*, 2013); (100× objective, AxioImager M2; Zeiss; counting frame: 50 × 50 µm, grid size: 200 × 200 µm; every fourth section was analysed). Counts were performed manually and blinded for experimental grouping. Fluorescent images were taken using an Olympus IX-81 microscope (Olympus). Exposure time was equal for the same staining across the experimental groups. Fibre density in the striatum was analysed as previously described (Szego *et al.*, 2012).

For visualization of TH-positive fibres in the striatum, we used nickel intensification of the TH-staining (without Nissl counterstaining), as described previously (Szego *et al.*, 2012). Briefly, sections were treated with anti-TH (rabbit polyclonal, 1:1000, Millipore) antibody for 48 h at 4°C, then treated with biotinylated anti-rabbit IgG (1:200; Vector Laboratories) followed by avidin–biotin–horseradish peroxidase (HRP) complex (Vector Standard Elite® Kit, 1:500). Peroxidase labelling was visualized by diaminobenzidine tetrahydrochloride.

For protein analysis, brains were quickly removed, striatum dissected and samples homogenized in RIPA buffer in the presence of protease and phosphatase inhibitors (Roche Complete and PhosStop). Samples were then rotated for 1 h at 4°C and centrifuged at 18 000 *g* for 30 min. For further analyses, we used the soluble fractions. α-Synuclein was partially purified and enriched as described (Vicente Miranda *et al.*, 2013). For immunoblotting, we used anti aSyn (BD Transduction laboratories, S63320, 1:3000), anti-CEL (Cosmobio, CAC-AGE-M02, 1:500) or anti-AGEs (Millipore, AB9890, 1:1000).

Animals used for electrophysiological studies

Wild-type male Wistar rats (8–12 weeks old) were obtained from Harlan Interfauna Iberica, SL. All procedures used in the present study complied with the European Community guidelines (86/609/EEC) and Portuguese law on Animal Care (1005/92). Environmental conditions were kept constant: food and water *ad libitum*, 21 ± 0.5°C, 60 ± 10% relative humidity, 12 h light/dark cycles.

Hippocampal slice preparation

Animals were anaesthetized under halothane atmosphere and sacrificed by decapitation. Brains were rapidly removed and the hippocampi were dissected free in ice-cold artificial CSF composed of (in mM): 124 NaCl, 3 KCl, 1.25 NaH_2PO4, 26 $NaHCO_3$, 1 $MgSO_4$, 2 $CaCl_2$, and 10 D-glucose, previously gassed with 95% O_2 and 5% CO_2, pH 7.4. Slices (400-µm thick) were cut transversally along the primary axis of the hippocampus with a McEwen tissue chopper and allowed to recover functionally and energetically for at least 60 min in a resting chamber immersed in the same solution, at room temperature (22–25°C) (Fredholm *et al.*, 1984). Slices were then incubated for 90 min either with vehicle, glycated α-synuclein (0.5 mM MGO for 30 h) or α-synuclein in gassed artificial CSF. The range of concentration chosen for α-synuclein incubation was based on previous data using 500 nM of different α-synuclein species (Diogenes *et al.*, 2012). All incubations were performed at room temperature to avoid neuronal damage by hypoxic injury (Schiff and Somjen, 1985). After this preincubation period, one slice was carefully deposited in a recording chamber for submerged slices and continuously superfused with gassed artificial CSF at a constant flow (3 ml/min) and temperature (32°C).

Evoked field synaptic potential recordings

Evoked field synaptic potentials (fEPSPs) were recorded through an extracellular microelectrode filled with 4 M NaCl (2–4 MΩ resistance) placed in the stratum radiatum of the CA1 area, as previously described (Diogenes *et al.*, 2011). The pathway of Schaffer collateral fibres was stimulated (rectangular pulses of 0.1 ms duration) once every 10 s by a bipolar wire electrode placed on the Schaffer fibres in the CA3 area. The initial intensity of the stimulus (200 µA) was adjusted to obtain a submaximal fEPSP slope with a minimum population

spike contamination, near one-third of the fEPSP slope obtained with supramaximal stimulation. The averages of eight consecutive fEPSPs from the Schaffer collateral CA1 pathway were obtained and quantified as the slope of the initial phase of the potential. Recordings were obtained with an Axoclamp 2B amplifier (Molecular Devices), digitized and continuously stored on a personal computer with the WinLTP program (Anderson and Collingridge, 2001).

Long-term potentiation induction

Long-term potentiation (LTP) was induced after obtaining a stable recording of fEPSP (each fEPSP is the average of eight individual fEPSPs) slope in the Schaffer collateral pathway for at least 30 min. LTP was induced by a theta-burst protocol (10 trains separated by 200 ms, four pulses each, 100 Hz) in the Schaffer collaterals/CA1 synapse. The intensity of the stimulus was kept constant throughout these induction protocols. LTP was quantified as the percentage of change in the average slope of the fEPSP taken from 46 to 60 min after LTP induction in relation to the average slope of the fEPSP measured during the 10 min that have preceded the induction of LTP.

Glycation studies in human tissue

Human brain fragments from Parkinson's disease, dementia with Lewy bodies, and control individuals were kindly provided by the Pathology Department, Hospital de Santa Maria and by Prof. Matthew Frosch from the Massachusetts Alzheimer's Disease Research Center. Protein samples were prepared as in Vicente Miranda *et al.* (2013). For immunoblotting, we used anti-aSyn (BD Transduction laboratories, S63320, 1:3000) and anti-CEL (Cosmobio, CAC-AGE-MG02, 1:500).

Mass spectrometry analysis

Total protein extracts from Δ*glo1* yeast expressing α-synuclein, H4 cells expressing α-synuclein treated with MGO (0.5 mM) and brain samples from B6D2F1 wild-type mice or Wistar wild-type rat were processed (Vicente Miranda *et al.*, 2013). Mass spectrometry was carried out on an Applied Biosystems 4700 Proteomics Analyzer with TOF/TOF ion optics as previously described (Vicente Miranda *et al.*, 2013). All peptide mass values were considered monoisotopic, a mass spectrometry mass tolerance was set at 100 ppm. Trypsin and endoproteinase Glu-C were assigned as digestion enzymes of α-synuclein. A triple miscleavage was allowed and oxidation of methionyl residues, acetylation of the N-terminal region, and carboxyethylation (CEL) of lysine residues were assumed as variable modifications. All peaks with $S/N > 5$ were included for matching against *in silico* digestion of corresponding α-synuclein sequence (*Homo sapiens*, *Mus musculus* or *Rattus*) in mMass software (Strohalm *et al.*, 2010).

α-Synuclein recombinant protein expression and purification

Escherichia coli BL21 (DE3) pLysS competent cells (Novagen) were transformed with human α-synuclein wild-type, A30P, A53T and E46K PT7-7 constructs. Expression and purification was performed as previously described (Vicente Miranda *et al.*, 2013) with the following changes: anion exchange was performed in HiTrap® Q XL and size exclusion in Superdex™ 200 10/300 (GE Heathcare). Protein concentration was determined by UV absorbance at 275 nm ($\varepsilon_{aSyn275} = 5600\,M^{-1}\,cm^{-1}$). For ^{15}N-labelling of α-synuclein wild-type, cells were grown in M9 medium supplemented with ^{15}N-labelled ammonium chloride.

Kinetics of α-synuclein fibril formation

Solutions of human recombinant α-synuclein (100 μM) were agitated at 37°C in the presence of MGO. Fibril formation was monitored with Thioflavin T (ThT) binding assay as previously described (Naiki *et al.*, 1989, 1990). Fluorescence measurements were performed using a Perkin Elmer LS50B spectrofluorometer, in quartz cuvettes with 1 cm excitation light path. ThT fluorescence was recorded immediately after ThT binding from 470 to 600 nm with excitation at 450 nm, an increment of 0.5 nm, an integration time of 1 s and 5 nm slits for both excitation and emission. For each sample, the signal was obtained as the ThT intensity at 482 nm from which was subtracted a blank measurement recorded prior to the addition of α-synuclein to the ThT solution.

Secondary structure kinetic analysis by circular dichroism

Secondary structure analysis of MGO-incubated α-synuclein was performed by far-UV (185–260 nm) circular dichroism (CD) in a Jasco J810 spectropolarimeter equipped with a temperature control unit Julabo F25. Far-UV CD spectra were recorded in solutions of 100 μM α-synuclein in a 0.01 cm (linear) path length quartz cuvette at 37°C in 50 mM potassium phosphate buffer, pH 7.4, with 150 mM of NaF. For each spectrum, three scans were averaged.

α-Synuclein oligomer formation analysis by size exclusion chromatography

Oligomerization of human α-synuclein upon methylglyoxal glycation was monitored by size exclusion chromatography (SEC). Solutions of monomeric α-synuclein treated with vehicle (PBS) or MGO (5 mM) were incubated and agitated at 37°C. Samples (50 μl at 100 μM) were analysed by SEC at defined incubation times, after filtration with a 0.2 μm Whatman filter. SEC was performed with HPLC Jasco PU-2080 Plus isocratic pump with a UV detector Jasco 2075. The mobile phase was 50 mM PBS pH 7.4 with 150 mM NaF. Separation was achieved on a molecular exclusion analytical column (GE-Healthcare Superdex 75 10/300 GL) at a flow rate of 0.4 ml/min. Eluting peaks were monitored at 275 nm.

α-Synuclein oligomer formation analysis by dynamic light scattering

Oligomer formation was monitored by dynamic light scattering as previously described (Martins *et al.*, 2008; Faustino

et al., 2014). Dynamic light scattering experiments performed on a Malvern Zetasizer Nano ZS with backscattering detection at 173°, equipped with a He-Ne laser (λ = 632.8 nm), using glass cuvettes with round aperture at 25°C. Agitated α-synuclein (30 h at 900 rpm), treated with Tris-buffer or MGO (0.5 mM) was diluted to 7 μM in Tris-buffer. Samples were allowed to equilibrate for 15 min at 25°C before each 10 measurements set (each set is the average of 10 runs, with 10 s per run). Each experiment was repeated at least three times. Data were evaluated in Zetasizer Nano ZS software (Malvern).

Nuclear magnetic resonance spectroscopy

MGO-glycation of α-synuclein was obtained by incubating 50 μM of protein with 4.6 molar excess of MGO in 20 mM sodium phosphate buffer pH 7.5. After 2.5 days of reaction at 15°C, buffer was exchanged to HEPES 25 mM pH 7.0 NaCl 50 mM. $^{1}H^{15}N$ HSQC spectra of wild-type and glycated ^{15}N-labelled α-synuclein samples were acquired at 15°C on a 600 MHz Bruker spectrometer, in HEPES 25 mM pH 7.0 NaCl 50 mM, 10% D_2O. α-Synuclein backbone resonance assignment was transferred from previous studies (Bertoncini *et al.*, 2005). In case of glycated α-synuclein, peak centre was adjusted only in regions of small signal overlap. Peaks affected by severe overlap were excluded from the analysis. Nuclear magnetic resonance (NMR) data were processed and analysed with NMRPipe (Delaglio *et al.*, 1995) and Sparky (T. D. Goddard and D. G. Kneller, University of California, San Francisco).

α-Synuclein binding studies to small unilamellar vesicles

Small unilamellar vesicles (SUVs) were prepared using 1-palmitoyl-2-oleoyl-sn-glycero-3-phosphocholine (POPC) and 1-palmitoyl-2-oleoyl-sn-glycero-3-phosphate (POPA) (Avanti Polar Lipids), at 1:1 molar ratio following the procedure described previously (Karpinar *et al.*, 2009). SUVs were prepared in HEPES 25 mM pH 7.0 NaCl 50 mM. Starting from 12.5 mM total lipid concentration, the SUVs, isolated after sonication and ultracentrifugation showed a hydrodynamic diameter of 25 ± 4 nm as determined by dynamic light scattering. Again, MGO-glycation of α-synuclein was obtained by incubating 50 μM of protein with 4.6 molar excess of MGO in 20 mM sodium phosphate buffer pH 7.5. After 2.5 days of reaction at 15°C, buffer was exchanged to HEPES 25 mM pH 7.0 NaCl 50 mM.

Far-UV CD spectra were recorded at 20°C using 1-mm length Hellma quartz cuvette in Chirascan (Applied Photophysics) spectrometer, with 0.5 nm bandwidth. Samples were measured at 7 μM protein concentration in 5 mM sodium phosphate buffer pH 7.0. To obtain the spectra of free and SUV-bound α-synuclein, measurements were done in triplicate and the contribution of buffer and vesicles to the CD signal was subtracted as appropriate.

Transmission electron microscopy

Aggregated α-synuclein (5 μl of 100 μM) treated with vehicle (PBS) or MGO (5 mM) was applied to carbon-coated Formvar 200 mesh grids (Electron Microscopy Sciences) and incubated at room temperature for 60 s. The grids were then washed sequentially by depositing 10 μl droplets of double distilled sterile water (twice) followed by a 10 μl droplet of fresh 2% (w/v) uranyl acetate, which remained on the grid for 30 s. After each step, the excess solution was blotted with Whatman® filter paper, and the grids were vacuum dried from the edges. The samples were analysed using a Phillips CM-10 TEM microscope operated at 100 kV acceleration voltage.

α-Synuclein clearance

For cycloheximide chase experiments, H4 cells were transfected as previously described (Vicente Miranda *et al.*, 2013) with pSI-aSyn plasmid. After 24 h, cells were treated with vehicle (H_2O) or MGO (0.5 mM) for 16 h. Media was renewed and cells rechallenged with vehicle or MGO for 24 h in the presence of cycloheximide (100 μM, added at given time points). Protein extracts were immunoblotted.

Proteasome impairment was assessed as the amount of unstable GFP (GFPu) accumulation. H4 cells were cotransfected with empty vector with GFPu; α-synuclein with GFPu or SynT with GFPu. Twenty-four hours post-transfection, media was renewed and cells treated with vehicle (H_2O) or MGO (0.5 mM) for 16 h and processed for immunoblotting with anti-GFP antibody (NeuroMab, P42212).

For autophagy impairment studies, H4 cells were transfected with empty vector, with α-synuclein or co-transfected with SynT together with Synph 1. Twenty-four hours post-transfection, media was renewed and cells treated for 16 h with vehicle (H_2O) or MGO (0.5 mM). Media was again renewed and cells were rechallenged with vehicle or MGO during autophagy blockage with ammonium chloride (20 mM) together with leupeptin (200 μM) for 2 h. Autophagy activity was measured as the amount of accumulated LC3-II after treatment with autophagy blockers as previously described (Macedo *et al.*, 2015). P62 basal levels were also assessed in cells treated with vehicle or MGO (0.5 mM) for 16 h. Then, the media was renewed and cells were treated again with vehicle or MGO for 4 h (SQSTM1 D-3, sc-28359, 1:3000).

For α-synuclein release studies, H4 cells, co-transfected with SynT and Synph 1 for 24 h were treated with MGO (0.5 mM) for 16 h. Media was renewed, and cells were again treated with MGO (0.5 mM) for 6 h, media collected, applied to a dot-blot system and immunoblotted with anti-α-synuclein by standard procedures.

In vitro ubiquitination assays

Recombinant α-synuclein was glycated *in vitro* as described above. Both glycated or non-glycated α-synuclein were incubated in a reaction mixture containing 40 mM Tris-HCl (pH 7.6), 5 mM $MgCl_2$, 2 mM DTT, 1 mM ATP-γ-S, 7.5 μg ubiquitin, 1 μM ubiquitin aldehyde, 100 ng E1 and 200 ng UbcH5b,

in the presence or absence of 500 ng SIAH-2. Samples were incubated at 37°C for 1 h, and the reaction was stopped by the addition of SDS sample buffer. Samples were immunoblotted and mono-ubiquitinated α-synuclein determined using an anti-α-synuclein antibody.

MGO scavengers treatment in H4 cells

Twenty-four hours after SynT and Synph 1 co-transfection, cells seeded at 20 000 cells/cm^2 in 35 mm imaging dishes (Ibidi) or seeded at 30 000 cells/cm^2 in 6-well plates (TPP) were treated with vehicle (H_2O), MGO (0.5 mM), aminoguanidine (100 or 250 μM), tenilsetam (100 or 250 μM) or co-treated with vehicle or MGO (0.5 mM) with aminoguanidine (250 μM) for 16 h. α-Synuclein clearance assays were also performed in the presence of aminoguanidine (250 μM) or tenilsetam (250 μM).

Treatment of *Drosophila* with aminoguanidine hydrochloride or tenilsetam

Aminoguanidine hydrochloride (SIGMA: 396494), dissolved in PBS, tenilsetam (Axon Medchem, Axon 1470) dissolved in dimethyl sulphoxide (DMSO), PBS or DMSO were added to standard maize media at the required doses (100 or 300 μM). Newly emerged flies were placed on the drug food and kept for 10 days changing them daily with freshly prepared food containing the compound. Climbing activity was assessed at Day 10.

Compliance with ethical standards

The human samples used in our study were obtained from the ADRC at MGH, Boston, so all ethical considerations were taken into account. Animal work was performed with the approval from the animal care committee of IMM, Lisbon, Portugal.

Results

MGO induces α-synuclein aggregation and toxicity in cell models of Parkinson's disease

First, we investigated the effect of MGO on α-synuclein aggregation and toxicity in yeast cells constitutively expressing α-synuclein (Outeiro and Lindquist, 2003). We modulated MGO levels, using either increased amounts of D-glucose in the media, or genetically, using *Glo1* (Δ*glo1*) or triose phosphate isomerase (*Tpi*) deletion (Δ*tpi*) strains, conditions known to increase the levels of MGO and promote the formation of AGEs (Gomes *et al.*, 2005; Guix *et al.*, 2009; Orosz *et al.*, 2009). We found that these glycation-promoting conditions increase MGO levels ~3-fold (Supplementary Fig. 1A). Glycating conditions increased both the percentage of cells with α-synuclein inclusions (Fig. 1A), and α-synuclein toxicity in Δ*glo1* and Δ*tpi* mutant cells expressing wild-type α-synuclein (Fig. 1B). Similar results were obtained with the Parkinson's disease-associated α-synuclein familial mutants A53T or E46K (Supplementary Fig. 1B and C). The increased toxicity upon glucose treatment was further confirmed by assessing yeast viability, and we observed a reduction in the number of CFUs (Supplementary Fig. 1D).

To further assess the effect of glycation on α-synuclein aggregation and toxicity, human H4 cells were co-transfected with an aggregation-prone variant of α-synuclein, known as SynT (full-length α-synuclein fused with the first 83 amino acids of GFP), together with synphilin-1 (Synph 1), an α-synuclein-interacting protein that potentiates α-synuclein aggregation (McLean *et al.*, 2001). As we previously reported, this model facilitates the visualization of α-synuclein inclusions that, in contrast with the expression of unmodified α-synuclein, does not form inclusions (Klucken *et al.*, 2012; Basso *et al.*, 2013; Guerreiro *et al.*, 2013; Lazaro *et al.*, 2014). We selected 0.5 mM MGO as the working concentration as it increased protein glycation without increasing overall cytotoxicity in naïve cells (Supplementary Fig. 2A–C). We found that this concentration, widely used in various studies (Nass *et al.*, 2014; Chang *et al.*, 2016; Hansen *et al.*, 2016), increased the levels of MGO ~1.4-fold (Supplementary Fig. 2D). Treatment with MGO resulted in a striking increase in the percentage of cells with inclusions (from ~51% to ~85%). We also observed an increase in the number of inclusions per cell (~17% to ~35% increase of cells displaying at least 10 inclusions, or ~34% to ~62% within cells with inclusions) (Fig. 1C). Although MGO induced cytotoxicity in empty vector transfected cells, MGO increased α-synuclein toxicity (2.5-fold versus vehicle treated SynT + Synph 1) (Fig. 1D), and induced both α-synuclein Triton^{TM} X-100 insolubility (3-fold versus control) (Fig. 1E), and the formation of high molecular weight species, as assessed in 5–30% sucrose gradients (Fig. 1F). The combination of MGO treatment in α-synuclein-expressing cells elicited a significant increase in cytotoxicity, but each insult alone was also cytotoxic. Therefore, it remains to be investigated whether the combination of both insults represents a synergistic effect. We also assessed whether MGO induced α-synuclein glycation. For this, we immunoprecipitated α-synuclein from cells expressing α-synuclein or from cells co-expressing SynT and Synph 1 after treatment with MGO (0.5 mM). Remarkably, we observed an increase in the levels of glycated α-synuclein or SynT (Fig. 1G). This was also observed in whole cell lysates, where the glycation levels of several proteins are increased upon treatment with MGO (Supplementary Fig. 2E), however, the levels of Synph 1 were not altered in glycating conditions (Supplementary Fig. 2F).

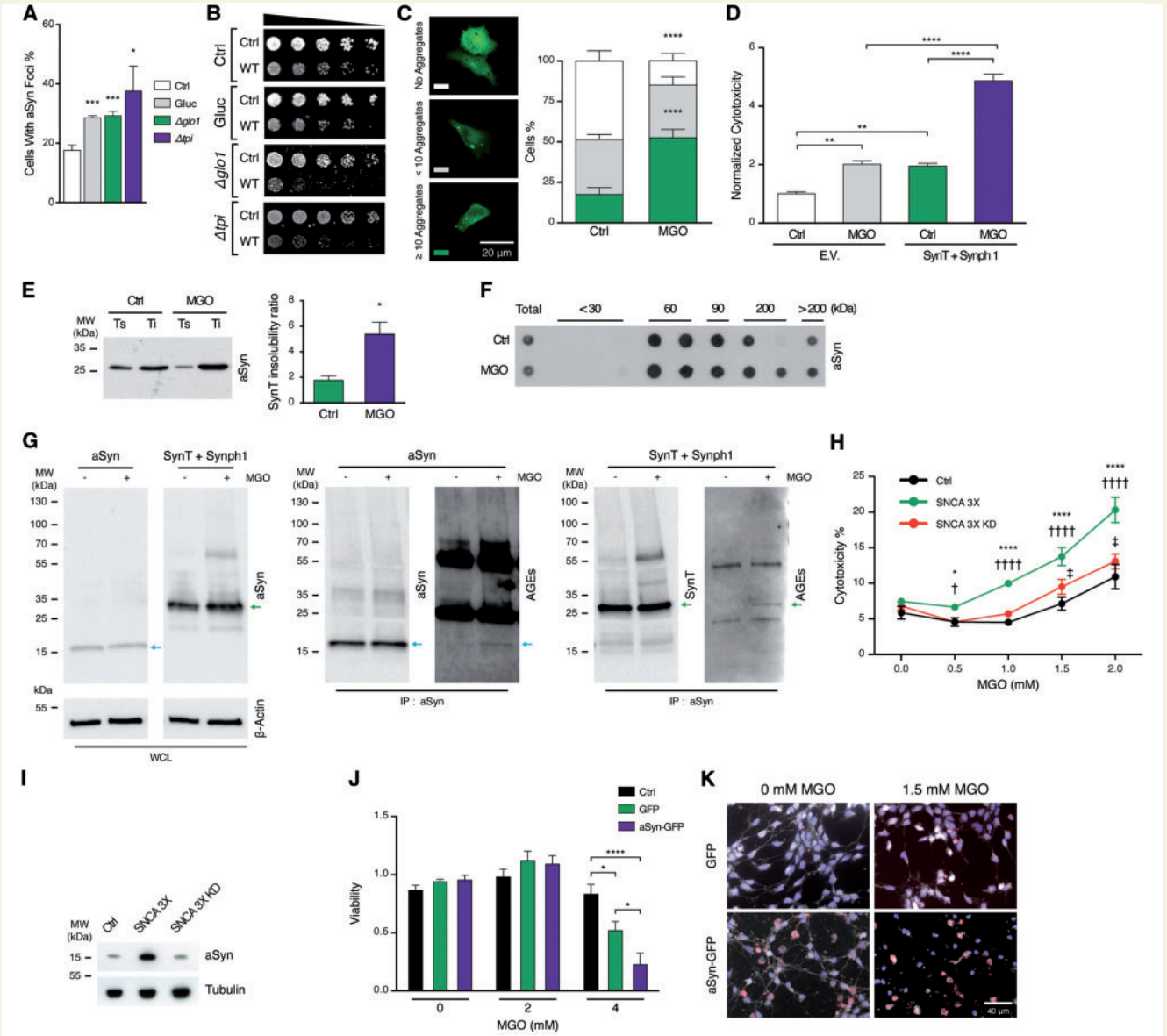

Figure 1 MGO induces α-synuclein aggregation and toxicity in yeast and mammalian cell models of Parkinson's disease. BY4741 wild-type reference strain and Δ*glo1* or Δ*tpi* yeast cells transformed with empty p426GPD vector (Ctrl) or with p426GPD-α-synuclein wild-type were grown in YNB-U. Cells were also grown in higher glucose concentrations (4%). (**A**) Percentage of yeast cells displaying α-synuclein inclusions. (**B**) Toxicity of α-synuclein under glycating conditions. (**C**) H4 cells co-expressing SynT and Synph 1 were treated with vehicle (Ctrl) or MGO (0.5 mM) for 16 h and processed for ICC (α-synuclein, green). Percentage of cells with aggregates ($n = 3$). (**D**) H4 cells co-transfected with empty vector (E.V.) or SynT and Synph 1 were treated with vehicle (Ctrl) or MGO (0.5 mM) for 16 h. MGO toxicity was measured by caspase-3 release ($n = 3$). (**E**) H4 cells, as in **C** were treated with vehicle (Ctrl) or MGO (0.5 mM) for 16 h. Triton™ X-100 soluble and insoluble (TS and TI) fractions were probed for α-synuclein. The ratio between soluble and insoluble fractions is presented as SynT insolubility ($n = 4$). (**F**) H4 cells, as in **C**, were treated with vehicle (Ctrl) or MGO (0.5 mM) for 16 h. Native protein extracts were separated in a sucrose gradient. Fractions were immunoblotted and probed for α-synuclein. (**G**) H4 cells were treated as in (**C**). Cells were lysed and immunoprecipitated (IP) with an antibody against α-synuclein. Whole cell lysates (WCL) were probed for α-synuclein and for the corresponding loading control (β-actin). Immunoprecipitated samples were probed for α-synuclein and AGEs. Blue and green arrows indicate α-synuclein and SynT, respectively ($n = 3$ times). (**H**) Patient-derived neuronal differentiated iPSCs from a family with a *SNCA* locus triplication (SNCA 3X), an age-matched healthy control (Ctrl) and an α-synuclein shRNA silenced cell line derived from the SNCA 3X (SNCA 3X KD) were treated with increasing concentrations of MGO (0–2 mM). MGO toxicity was measured by the activity of released LDH, normalized to total cell death ($n = 3$), and is displayed as per cent of cytotoxicity. (**I**) Protein extracts collected from iPSCs from Ctrl, SNCA 3X and SNCA 3X KD lines were immunoblotted with anti-α-synuclein and anti-tubulin antibodies. (**J**) Differentiated LUHMES cells, naive (Ctrl), stably expressing only GFP, or α-synuclein and GFP were treated with increasing concentrations of MGO (0–5 mM). MGO toxicity was assessed by the MTS assay ($n = 3$). (**K**) Cells stably expressing GFP or α-synuclein treated with vehicle (PBS) or 1.5 mM MGO were processed for immunocytochemistry (ICC) and stained for α-synuclein (white), Caspase 3 (red) and DNA (blue). Scale bar = 40 µm. Data in all panels are average ± SD, $^{*}P < 0.05$, $^{**}P < 0.01$, $^{***}P < 0.001$, $^{****}P < 0.0001$. For **A**, unpaired two-tailed *t*-test with equal SD; for **C** and **D**, two-way ANOVA, followed by Tukey's multiple comparisons test; for **E**, unpaired two-tailed *t*-test with equal SD. For **H**, SNCA 3X versus Ctrl $^{****}P < 0.0001$; SNCA 3X versus SNCA 3X KD $^{\dagger}P < 0.05$, $^{\dagger\dagger\dagger\dagger}P < 0.0001$; and SNCA 3X versus Ctrl $^{\ddagger}P < 0.05$, two-way ANOVA, followed by Tukey's multiple comparisons test. For **J**, two-way ANOVA, followed by Tukey's multiple comparisons test. aSyn = α-synuclein.

MGO induces α-synuclein toxicity in dopaminergic-neural induced pluripotent stem cells and dopaminergic-LUHMES cells

We next asked whether the correlation between α-synuclein expression and MGO-induced toxicity was conserved in human neurons. For this, we evaluated the effects of MGO in two different dopaminergic (DA) cell models: differentiated human DA-neural iPSCs and LUHMES. IPSCs, derived from dermal fibroblasts from a patient carrying a triplication of the *SNCA* locus and from an age-matched healthy relative (Byers *et al.*, 2011), were cultured and differentiated into DA neurons according to established protocols (Mak *et al.*, 2012; Oliveira *et al.*, 2015). LUHMES cells transduced with lentiviruses encoding α-synuclein-IRES-GFP or IRES-GFP, were differentiated into TH-positive neurons (DA-LUHMES) (Scholz *et al.*, 2011). Both types of human cells were treated with increasing concentrations of MGO. We observed a dose-dependent increase in MGO toxicity in terminally differentiated iPSCs carrying the *SNCA* gene triplication (SNCA 3X) (Fig. 1H) (Byers *et al.*, 2011). To determine whether toxicity was indeed associated with the expression of α-synuclein, we knocked down α-synuclein using shRNA (SNCA 3X KD) as in (Oliveira *et al.*, 2015) (Fig. 1I). This reduced MGO-induced toxicity (Fig. 1H), confirming the interplay between MGO and α-synuclein. Likewise, DA-LUHMES cells expressing α-synuclein were more sensitive to MGO compared both to GFP-expressing and to non-transduced cells (Fig. 1J), as observed through the appearance of dystrophic processes (Fig. 1K). Together, these results revealed a strong connection between increased levels of α-synuclein and glycating conditions.

Glycation decreases motor performance, lifespan and survival in *Drosophila*

We next asked whether MGO-induced α-synuclein toxicity affected motor performance. To address this, we used an established *Drosophila* model of Parkinson's disease based on the pan-neuronal expression of human α-synuclein via the GAL4/UAS system (Feany and Bender, 2000) and interrogated whether genetic modulation of glycation, via knockdown of *Glo1* or *Tpi*, altered α-synuclein-induced defects. We previously observed that knockdown of *Glo1* or *Tpi* increases the overall levels of glycation (Vicente Miranda *et al.*, 2016*b*), a phenotype that was also confirmed in this study (Fig. 2A). Importantly, we observed that knockdown of *Glo1* or *Tpi* alone did not elicit neurodegeneration, as assessed by counting the number of rabdomeres (photoreceptors) (Vicente Miranda *et al.*, 2016*b*). Here, we observed that α-synuclein expression significantly impaired motor performance (measured as climbing ability, due to negative geotaxis) of the flies and, importantly, when α-synuclein was expressed in the RNAi lines, the climbing impairment was aggravated (Fig. 2B, C and Supplementary Fig. 3A). Nevertheless, *Tpi* or *Glo1* knockdown also elicited a climbing impairment *per se*.

In addition, the maximal lifespan in *Glo1* knockdown reduced 2 days (comparing to non-silenced α-synuclein expressing flies) (Fig. 2D). Although silencing of *Tpi* shortened the lifespan by 4 days in both wild-type flies and α-synuclein expressing flies (Fig. 2E), we observed a striking decrease in survival starting 6 days post-eclosion (by Day 13, 77 ± 4% versus 93 ± 3%) survival for α-synuclein expressing flies (Fig. 2E and Supplementary Fig. 3B).

Glycation induces neuronal loss in a mouse model of Parkinson's disease and impairs synaptic transmission in brain slices

Next, to determine whether glycation modulates α-synuclein toxicity in the brain *in vivo*, we evaluated the effects of MGO in transgenic mice expressing human α-synuclein under the control of the *Thy1* promoter. We injected MGO and PBS in the two hemispheres (in the substantia nigra or striatum) of α-synuclein transgenic or wild-type control mice. Immunohistochemical analyses revealed a marked decrease in the number of TH-positive neurons in the MGO-injected side of the α-synuclein transgenic mice, when compared to the PBS-injected side (Fig. 3A). Neuritic degeneration was also evident in the striatum, where the terminals of the nigral TH-positive neurons are located (Fig. 3A). Remarkably, we detected high levels of CEL immunoreactivity only in the MGO-injected substantia nigra of α-synuclein transgenic mice, but not in the MGO-injected wild-type control substantia nigra (Fig. 3B). Stereology analyses showed that injection of MGO induced a 32.9 ± 3.5% loss of TH-positive neurons, a 46 ± 5.1% loss of VMAT-, and a 43.0 ± 3.0% loss of DAPI-positive neurons (as a percentage of the PBS-injected side, compared to 9.6 ± 5.7; 9.7 ± 3.4, and 5.8 ± 7.4% loss of TH-, VMAT- or DAPI-positive neurons in wild-type mice, respectively) (Fig. 3C). We should highlight that the results shown do not simply correspond to the total number of labelled neurons (TH, VMAT or DAPI), but to the percentage of neurons normalized to the corresponding control (MGO/PBS in wild-type mice, black bars; or MGO/PBS in α-synuclein transgenic mice, green bars in Fig. 3C). Immunostaining for TH in coronal sections (revealed with DAB) confirmed that TH-positive neuronal loss was specifically observed in α-synuclein transgenic mice injected with MGO (Supplementary Fig. 4A). When MGO was injected in the striatum, we also found a significant loss of NeuN-positive neurons in α-synuclein transgenic animals (13.5 ± 3.9%), while wild-type animals were almost unaffected (3.7 ± 1.7%) (Supplementary Fig. 4B). In addition, striatal TH fibre density was reduced in both the α-synuclein

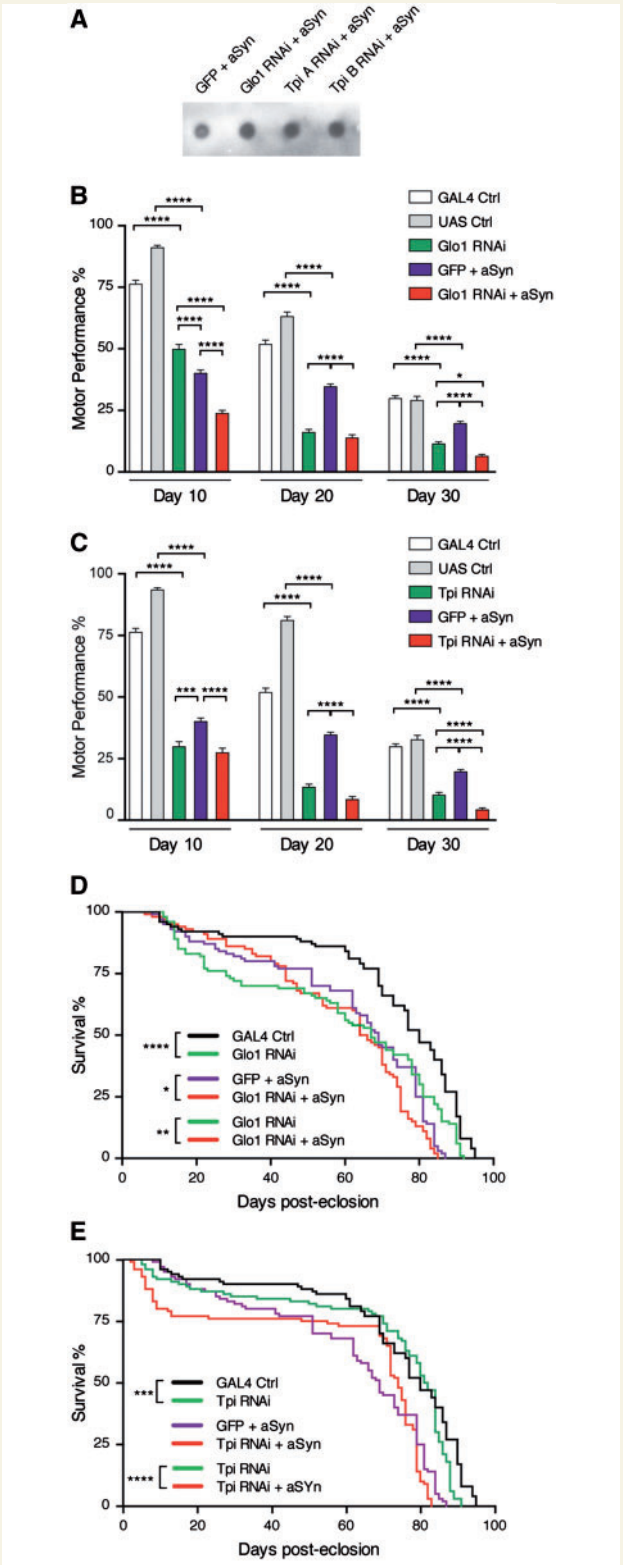

Figure 2 Downregulation of *Glo1* and *Tpi* increases glycation and impairs negative geotaxis and lifespan in flies. (**A**) Protein extracts from *Drosophila* heads were immunoblotted and probed for CEL. Silencing of *Glo1* and *TPI* increases protein glycation. *Drosophila* motor performance assessed as percentage of flies climbing more than 8 cm within 10 s. RNAi silencing of *Glo1* (**B**) and *Tpi* (**C**) caused a reduction in climbing behaviour in both wild-type and α-synuclein flies when compared to the respective controls (*n* = 50 per condition). Survival rate was evaluated in flies with pan-neuronal knockdown of *Glo1* (**D**) and *Tpi* (**E**) in wild-type and α-synuclein backgrounds (*n* = 100 per genotype). GAL4 Ctrl and UAS Ctrl data are common between panels. Data in all panels are mean ± SEM, $^{*}P < 0.05$, $^{**}P < 0.01$, $^{****}P < 0.0001$; for **B** and **C**, two-way ANOVA, followed by Tukey's multiple comparisons test; for **D** and **E**, Kaplan–Meier survival curve analysis with log-rank test. aSyn = α-synuclein.

transgenic and wild-type control animals, but was much more pronounced in α-synuclein transgenic mice (18.6 ± 4.1 versus 7.1 ± 2.2%) (Supplementary Fig. 4B).

To establish whether MGO also promoted α-synuclein glycation, we enriched α-synuclein from striatal-injected extracts (Vicente Miranda *et al.*, 2013) and measured the levels of CEL, the AGE derived from the reaction of MGO with lysine residues of proteins (Ahmed *et al.*, 1997), on α-synuclein. Since we showed by immunoprecipitation that α-synuclein was glycated and that glycated α-synuclein migrated with an identical molecular weight to that of α-synuclein (Fig. 1G), we assumed that the CEL protein band overlapping with α-synuclein, corresponded to glycated α-synuclein. Upon quantification, we found that α-synuclein glycation increased ∼2-fold in MGO-injected α-synuclein transgenic animals (Fig. 3D).

Interestingly, we found high reactivity against aggregated α-synuclein in the substantia nigra of the MGO-injected α-synuclein transgenic mice (Fig. 3E). By analysing higher magnifications of substantia nigra sections, we observed aggregated α-synuclein both in cell bodies and neuronal processes (Supplementary Fig. 5A). In addition, we found stronger staining against phosphorylated α-synuclein (serine 129 phosphorylation, pS129) in the substantia nigra of MGO-injected α-synuclein transgenic mice (Supplementary Fig. 5B) indicating increased α-synuclein pathology. pS129 signal was specifically present in surviving TH-positive neurons in MGO-injected α-synuclein transgenic mice as well (Supplementary Fig. 5C).

Immunohistochemistry for α-synuclein in mice injected in the striatum revealed presynaptic staining for both wild-type and α-synuclein transgenic mice. However, in α-synuclein transgenic mice treated with MGO, α-synuclein was also found in cell bodies. Importantly, staining with methoxy-XO4 (MX), an amyloid-binding dye (Klunk *et al.*, 2002), revealed amyloid-like inclusions adjacent to the MGO injection site in the α-synuclein transgenic mice (Supplementary Fig. 5D).

To assess whether glycation induced functional alterations on synaptic transmission, we used a paradigm based on the treatment of hippocampal brain slices with α-synuclein oligomeric species (Diogenes *et al.*, 2012). We found that α-synuclein that was previously glycated with MGO strongly impaired synaptic plasticity in the rat hippocampus (LTP_{aSyn} 47 ± 3%; $LTP_{aSyn\text{-}MGO}$ 22 ± 4%) (Fig. 3F–I). Importantly, PBS or MGO (35 μM) treatment did not affect LTP (Supplementary Fig. 6).

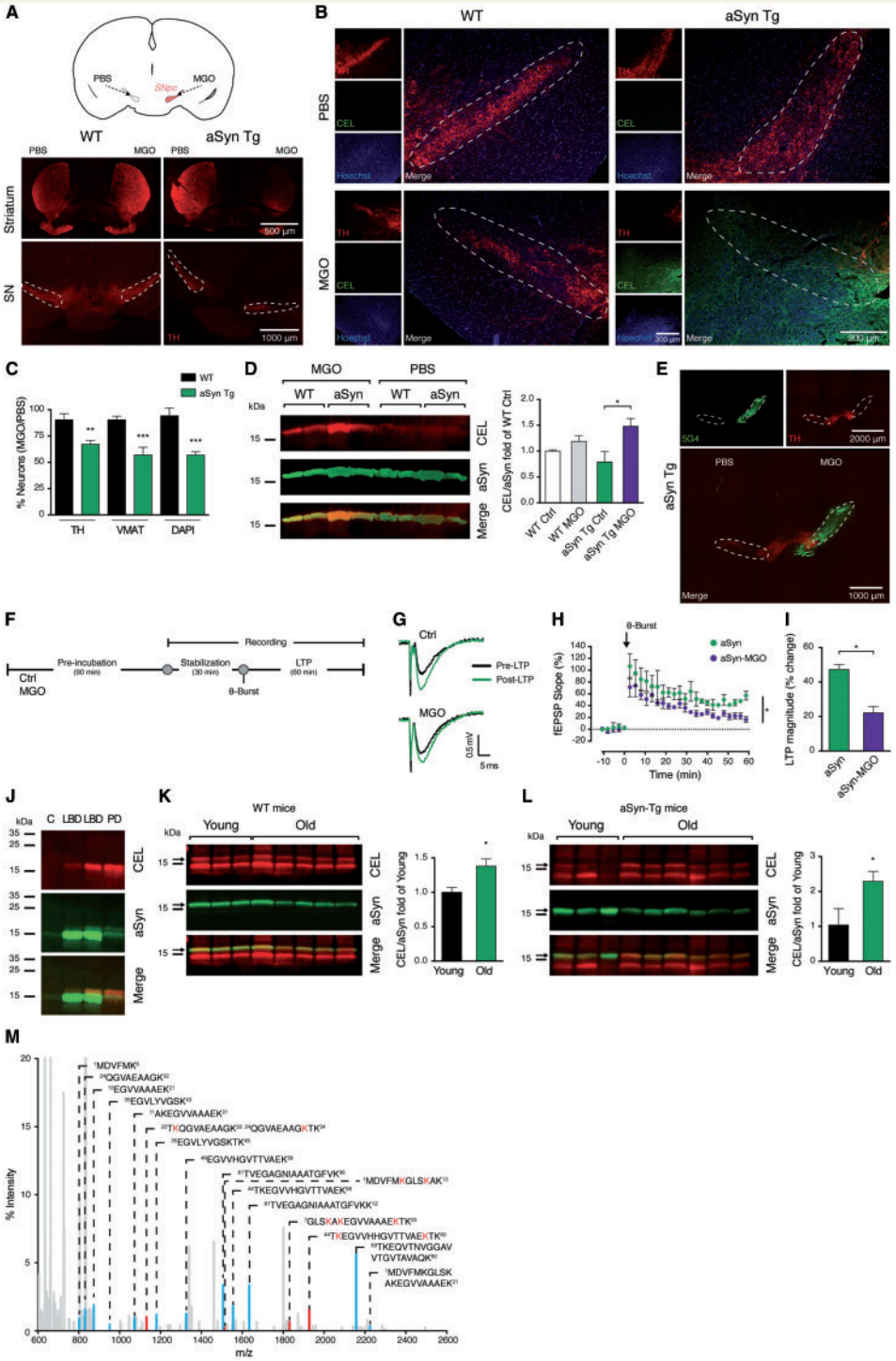

Figure 3 MGO is neurotoxic in mice, induces α-synuclein glycation and aggregation, and impairs synaptic transmission. Wild-type (WT) and α-synuclein transgenic (Tg) mice were injected in the substantia nigra (SN, schematic view) either with MGO or vehicle (PBS) and analysed 7 days post-injection. (**A**) Representative micrographs of brain sections immunostained for TH (red). Scale bar = 500 µm and 1000 µm for striatum and substantia nigra, respectively. Dashed line delineates the area corresponding to the substantia nigra. (**B**) Representative micrographs of brain sections immunostained for TH (red), CEL (green) or stained with Hoechst (blue). Scale bar = 300 µm. The merged signal is also shown. Scale bar = 200 µm. The dashed line delineates the substantia nigra. (**C**) The percentage of TH-, VMAT- or DAPI-positive cells (ratio MGO/PBS) is presented (at least $n = 3$ per condition). (**D**) Striatal thermo-enriched protein extracts were probed with anti-CEL (red) and anti-α-synuclein (green, samples from two animals are shown). Representative blots are shown. The ratio between CEL and α-synuclein is shown as CEL/α-synuclein fold of wild-type contralateral (Ctrl) (at least $n = 3$ per condition). (**E**) Representative image of brain sections immunostained for aggregated α-synuclein (5G4, green) and TH (red). Scale bar = 2000 µm for isolated channels and 1000 µm for merge. (**F**) Experimental setup for long-term potentiation. Rat hippocampal slices were preincubated for 90 min with α-synuclein (500 nM) treated with PBS (Ctrl) or MGO. The slices were allowed to stabilize for 30 min before θ-burst. (**G**) Traces from representative experiments shown in **H** obtained before and 46–60 min after LTP induction, composed of the stimulus artefact

(continued)

α-Synuclein is glycated in human brains and increases with ageing in mice

To assess the relevance of α-synuclein glycation in Parkinson's disease and other synucleinopathies further, we analysed the glycation pattern of α-synuclein in extracts from the cortex from human brain tissue enriched for α-synuclein (Vicente Miranda *et al.*, 2013). Using the previous assumption, we observed that samples derived from both control individuals, without overt symptoms of neurological disorders, and from individuals diagnosed with Parkinson's disease or Lewy body dementia, showed reactivity for CEL. Strikingly, α-synuclein was also reactive for this modification (Fig. 3J).

To establish whether this modification varied with ageing, as we predicted, we analysed brain samples from wild-type mice or human α-synuclein BAC transgenic mice at different ages. In transgenic mice, the expression of human α-synuclein is controlled by the human promoter, thereby avoiding possible confounding issues associated with α-synuclein overexpression. Importantly, we observed that α-synuclein was reactive for CEL (overlapping signal), and that this reactivity increased with age in both wild-type (~1.3-fold increase in old versus young animals) and α-synuclein BAC transgenic mice (2.3-fold increase in old versus young animals) (Fig. 3K and L).

Glycation occurs mainly in the N-terminal region of α-synuclein

Given that α-synuclein was found to be glycated in human brain and in mouse models, we sought to identify where glycation occurred in α-synuclein. For this, we used a proteomic approach (Vicente Miranda *et al.*, 2013). Briefly, we used mass spectrometry to analyse α-synuclein-enriched protein extracts from yeast Δ*glo1* cells expressing human α-synuclein, from human H4 cells expressing human α-synuclein treated with 0.5 mM MGO, and from mouse and rat brain tissues. By matching the mass spectrometry data with the m/z ratios calculated from *in silico* digested α-synuclein sequences (including CEL as variable post-translational modification), we found that α-synuclein was mainly glycated in the N-terminal region (K6, K10, K12, K21, K23, K32, K34 and K43 and K45) in all samples analysed (Fig. 3M, Supplementary Fig. 7 and Supplementary Tables 1–16), hinting at possible effects on membrane binding and aggregation.

MGO promotes α-synuclein oligomerization and impairs lipid binding ability

MGO glycation was previously shown to interfere with amyloidogenesis by stabilizing intermediate species (Lee *et al.*, 2009; Oliveira *et al.*, 2011; Padmaraju *et al.*, 2011). Thus, we investigated whether MGO affected the aggregation of wild-type and of three mutant variants associated with familial Parkinson's disease (A30P, E46K, and A53T). In agreement with our previous findings (Oliveira *et al.*, 2011, 2013), we found that, although glycation decreased α-synuclein fibril formation *in vitro* (Fig. 4A and Supplementary Fig. 8A–C), it potentiated the formation of α-synuclein oligomeric species, as observed by size exclusion chromatography analyses of MGO-treated versus non-treated α-synuclein (30 h of fibrillization). We found that oligomeric α-synuclein species were only present in samples with MGO (elution at 28 and 18 min) (Fig. 4B–D and Supplementary Fig. 8D). Consistently, analysis of the particle size distribution by dynamic light scattering, revealed a more heterogeneous size distribution of glycated α-synuclein, with a significant increase in particles with a hydrodynamic diameter above 2300 nm (Fig. 4C and D). Moreover, using transmission electron microscopy, we observed that vehicle-treated α-synuclein formed typical amyloid fibrils, whereas glycated α-synuclein formed amorphous aggregates and ring-shaped particles (Fig. 4E), consistent with α-synuclein oligomers (Lashuel *et al.*, 2002*a*, *b*).

To assess the effects of glycation on the structure of α-synuclein, we performed NMR analyses. We found that glycation induced a 76% reduction of the NMR backbone $^{1}H^{15}N$ signals up to residue 64, demonstrating the N-terminal region of α-synuclein was the most affected (Fig. 4F and G). The N-terminal domain of α-synuclein is involved in lipid-binding (Jo *et al.*, 2000). Interestingly, we observed that glycation impaired the typical transition between

Figure 3 Continued

followed by the presynaptic volley and the fEPSP. (**H**) Changes in fEPSP slope induced by θ-burst stimulation were recorded from the CA1 region of hippocampal slices pretreated with α-synuclein or with glycated α-synuclein (aSyn-MGO) (α-synuclein 47 ± 3%, $n = 4$; aSyn-MGO 22 ± 4%, $n = 4$). (**I**) Bar graph of the LTP magnitude (change in fEPSP slope at 50–60 min) in relation to pre-θ-burst values (100%) from experiments shown in **H** as indicated below each column ($n = 4$). Thermo-enriched brain samples from Parkinson's disease, Lewy body disease (LBD), or from control (C) individuals (**J**), or from young or old wild-type (**K**) or α-synuclein-transgenic mice (**L**) were probed with anti-CEL (red) and anti-α-synuclein (green). Arrows indicate α-synuclein molecular weight. The ratio between CEL and α-synuclein is shown as the CEL/α-synuclein ratio in young versus old mice. (**M**) Detection of lysine glycation sites in α-synuclein by peptide mass fingerprinting analysis of α-synuclein protein in total lysates from Thy1-α-synuclein transgenic mouse brain. The spectrum shows glycated α-synuclein peptides in red and other α-synuclein peptides in blue. Corresponding peptide sequences are illustrated (residues in red are glycated). For **C** and **D**, data are presented as average ± SD. For **C**, **D**, **I**, **K** and **L**, $^{*}P < 0.05$, $^{**}P < 0.01$, $^{***}P < 0.001$. For **C**, two-way ANOVA, followed by Tukey's multiple comparisons test. For **D**, one-way ANOVA, followed by Tukey's multiple comparisons test. Data in **H** and **I** are mean ± SEM. For **H** and **I**, one-way ANOVA test, followed by a Bonferroni's multiple comparison *post hoc* test. For **K** and **L**, unpaired *t*-test with equal SD. PD = Parkinson's disease.

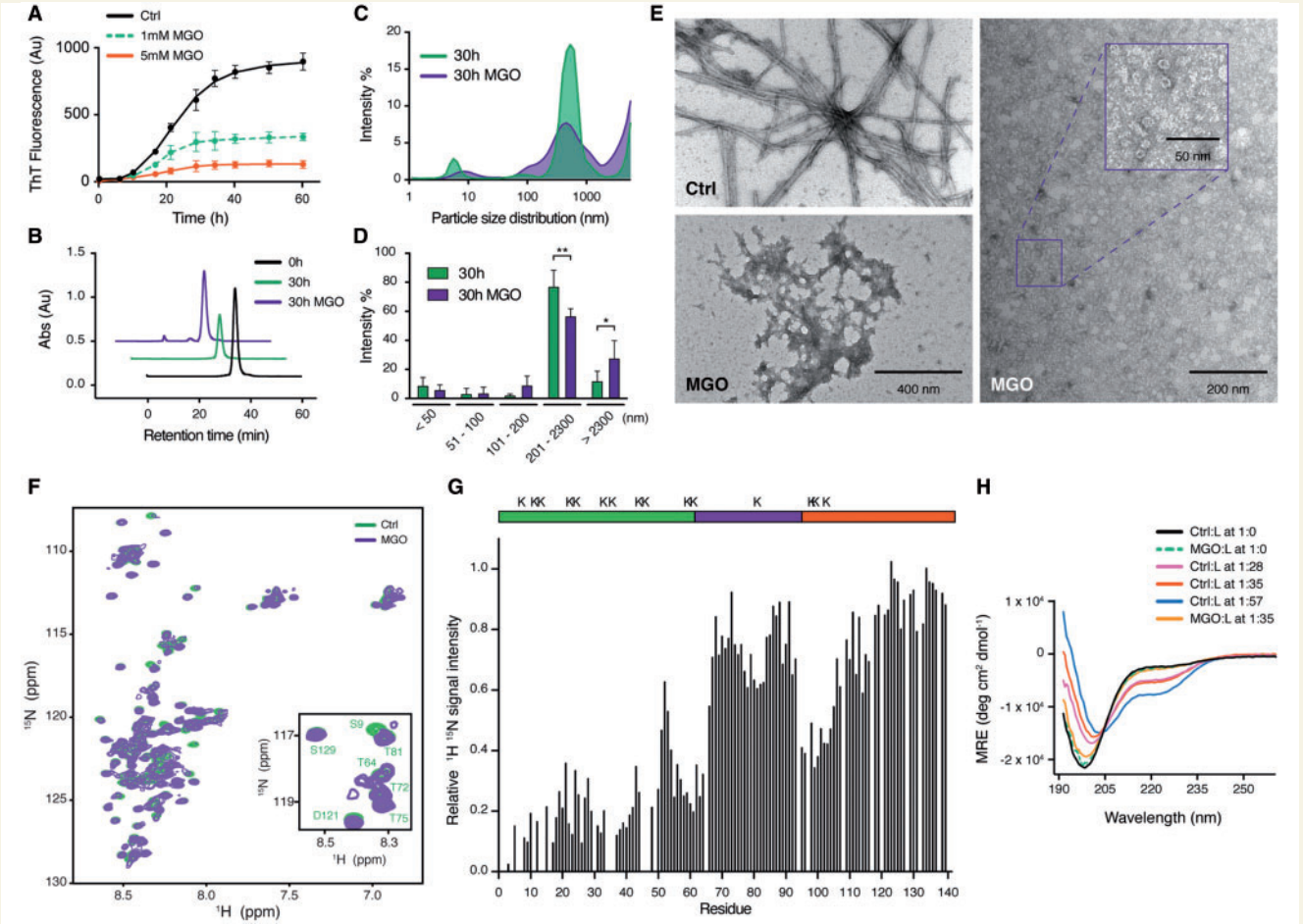

Figure 4 ***In vitro*** **MGO-glycation promotes α-synuclein oligomerization and impairs α-synuclein SUV binding.** (**A**) Fibrillization of recombinant wild-type α-synuclein at 100 μM treated with vehicle (Ctrl, black) or MGO (1 mM, green; and 5 mM, red) was followed by ThT fluorescence. (**B**) Recombinant wild-type α-synuclein species at 100 μM before (0 h, black) and after 30 h of fibrillization treated with vehicle (30 h, green) or MGO at 1 mM (30 h MGO, purple) were analysed by size exclusion chromatography. (**C**) Recombinant wild-type α-synuclein at 70 μM treated with vehicle (30 h) or MGO at 0.5 mM (30 h MGO) was fibrillized for 30 h and analysed by dynamic light scattering. Size (hydrodynamic diameter) distributions plotted as a function of scattered light intensity percentage ($n = 3$ for 30 h and $n = 4$ for 30 h MGO). (**D**) Dynamic light scattering size distributions by classes presented as scattered light intensity percentage. (**E**) Recombinant wild-type α-synuclein at 100 μM after 72 h of fibrillization treated with vehicle (Ctrl) or MGO (5 mM) was analysed by transmission electron microscopy (*left*, scale bar = 400 nm). A higher magnification of glycated α-synuclein is presented on the *right*. Scale bar = 200 nm. Red square outlines digitally magnified region. Scale bar = 50 nm. (**F**) Superposition of 2D $^{1}H^{15}N$ HSQC NMR spectra of recombinant ^{15}N-labelled α-synuclein before (green) and after (purple) treatment with MGO. Inset shows a selected region showing the glycation-induced NMR signal perturbation. (**G**) Residue-specific changes of $^{1}H^{15}N$ HSQC signal intensity of α-synuclein upon MGO glycation. Schematic of α-synuclein highlighting the N-terminal (green), NAC (purple) and C-terminal (red) domains, and location of lysine residues (**K**). (**H**) Far-UV CD spectra of unmodified (Ctrl) and glycated α-synuclein (MGO) in the absence and presence of POPC/POPA (1:1) SUVs at different protein-to-lipid (L) molar ratios.

random-coil and α-helical structure, which occurs when α-synuclein binds to SUVs (Fig. 4H).

Glycation blocks α-synuclein ubiquitination and impairs its clearance and release

As described above, we found that α-synuclein was glycated in the N-terminal region (Fig. 3M, Supplementary Fig. 7 and Supplementary Tables 1–16). Interestingly, several of those lysine residues are also known α-synuclein ubiquitination sites (Nonaka *et al.*, 2005; Anderson *et al.*, 2006). We hypothesized that if α-synuclein is glycated this might impair its normal ubiquitination and clearance. To investigate the mechanism through which MGO glycation potentiated α-synuclein-associated pathologies, we used a human cell model of α-synuclein aggregation (H4 cells, SynT-Synph 1 model). Strikingly, while we observed several ubiquitin and α-synuclein-positive inclusions in vehicle treated cells (as in Lewy bodies), no co-staining was observed in MGO-treated cells (Fig. 5A). To confirm that glycation competed ubiquitination, we performed an *in vitro* assay using SIAH-2, an E3 ubiquitin ligase known to ubiquitinate α-synuclein. We

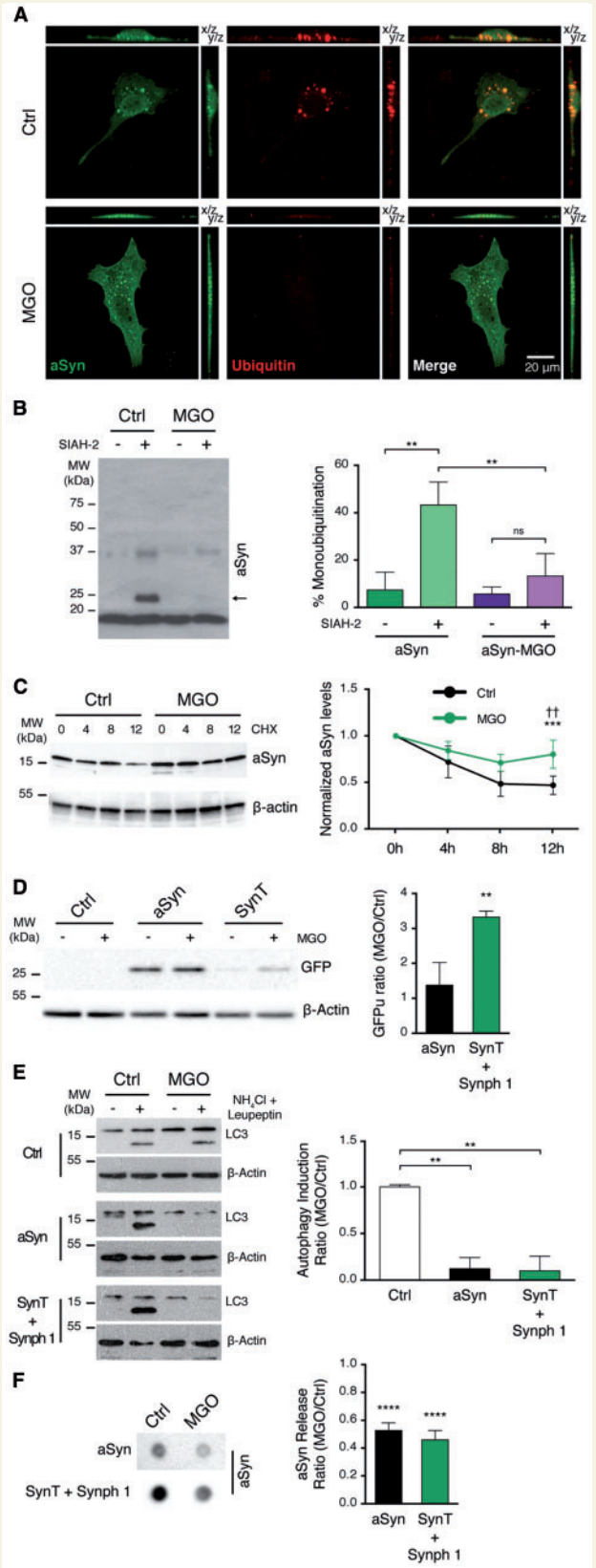

Figure 5 Glycation impairs α-synuclein clearance through the proteasome and autophagy and reduces α-synuclein release. (**A**) H4 cells expressing SynT and Synph 1 for 24 h were treated with vehicle (Ctrl) or MGO (0.5 mM) and stained for α-synuclein and ubiquitin. Micrographs of XY, YZ and XZ maximum intensity projections are shown. Scale bar = 20 µm. (**B**) *In vitro* α-synuclein ubiquitination reactions (of glycated or non-glycated α-synuclein) were conducted in the absence or presence of SIAH2. Mono-ubiquitination of α-synuclein was detected by immunoblotting against α-synuclein and represented as percentage of mono-ubiquitinated α-synuclein versus total α-synuclein. (**C**) Cells co-expressing SynT and Synph 1 were pretreated with vehicle (Ctrl) or MGO (0.5 mM) for 16 h. Cells were treated with vehicle or MGO for 24 h together with cycloheximide for the last 4, 8 or 12 h. Protein extracts were probed for α-synuclein and β-actin, for normalization. (**D**) Empty vector and GFPu (Ctrl), α-synuclein and GFPu (α-synuclein) or SynT and GFPu (SynT) cells were treated with vehicle (−) or MGO (0.5 mM) (+) for 16 h. Protein extracts were probed for GFP and β-actin. GFP signal was normalized to β-actin signal and to α-synuclein. The ratio between the levels of GFPu in cells treated with MGO or vehicle is presented. (**E**) Empty vector (Ctrl), α-synuclein or SynT + Synph 1 expressing cells were pretreated with vehicle (Ctrl) or MGO (0.5 mM) for 16 h. Cells were treated with vehicle or MGO for 2 h together with vehicle (−) or NH_4Cl and leupeptin (+). Protein extracts were probed for LC3 and β-actin. LC3-II levels were normalized to β-actin and the difference between NH_4Cl and vehicle treatments was calculated. The ratio between MGO and Ctrl is presented as autophagy induction ratio. (**F**) α-synuclein or SynT + Synph 1 expressing cells were treated with vehicle (Ctrl) or MGO (0.5 mM) for 16 h. Media was collected and probed for α-synuclein. Data are presented as MGO fold to Ctrl. See Supplementary Video 1. Data in all panels are average ± SD, $^{*}P < 0.05$, $^{**}P < 0.01$, $^{****}P < 0.0001$. For **B** and **E**, one-way ANOVA, followed by Tukey's multiple comparison test; for **C**, two-way ANOVA, followed by Sidak's multiple comparison test; for **D** and **F**, unpaired two-tailed *t*-test with equal SD. aSyn = α-synuclein.

observed that mono-ubiquitination of α-synuclein was reduced from 43 to 13% (Fig. 5B).

Next, we followed the clearance of α-synuclein in cells upon blocking *de novo* protein synthesis with cycloheximide. Importantly, we found that MGO treatment reduced α-synuclein clearance (Fig. 5C). To further dissect the effects of glycation on α-synuclein clearance, we investigated the activity of known α-synuclein clearance pathways (Ebrahimi-Fakhari *et al.*, 2012). First, to assess the effects on the ubiquitin proteasome system (UPS), we used an unstable version of GFP (GFPu) that reports on the overall activity of the UPS (Bence *et al.*, 2001). In control cells, no accumulation of GFP was observed. Upon α-synuclein expression, GFP accumulated in both vehicle and MGO-treated cells but the levels were ~2.5-fold higher in MGO versus PBS-treated cells (Fig. 5D). Together, our data indicate that UPS impairment is potentiated when α-synuclein is glycated.

Second, to study the effect of glycation on the autophagy-lysosome pathway, we treated cells with a combination of ammonium chloride (NH_4Cl) and leupeptin, known blockers of autophagy, according to established guidelines (Klionsky *et al.*, 2016). We observed that MGO severely decreased LC3-II levels in either α-synuclein or SynT expressing cells (~90% decrease) (Fig. 5E). Consistently, we found that the basal levels of P62 were increased

(Supplementary Fig. 9A). These data indicate that glycation impairs the autophagy-lysosome pathway.

Finally, as α-synuclein can be released from cells (Marques and Outeiro, 2012), we assessed whether this could also be affected by glycation. Interestingly, we found a significant reduction in α-synuclein release in cells treated with MGO (~50% decrease), therefore contributing to the intracellular accumulation of α-synuclein (Fig. 5F).

MGO scavengers correct the clearance of α-synuclein, reduce aggregation and toxicity, and alleviate motor phenotypes in *Drosophila*

Anti-MGO drugs such as aminoguanidine and tenilsetam are known scavengers of MGO (Webster *et al.*, 2005). Thus, we asked whether MGO scavenging could interfere with α-synuclein aggregation and toxicity. Importantly, both MGO scavengers reduced the intracellular levels of MGO by ~20% (Fig. 6A), resulting in a decrease of α-synuclein aggregation and toxicity by 20 and 50%, respectively (Fig. 6B and C). In addition, treatment with either aminoguanidine or tenilsetam reverted the impairment of α-synuclein clearance upon glycation (Fig. 6D and Supplementary Fig. 9B).

To assess the therapeutic potential of aminoguanidine and tenilsetam further, we tested their effect *in vivo*, using *Drosophila*. Strikingly, treatment with aminoguanidine or tenilsetam for 10 days improved the motor performance of α-synuclein expressing flies in a dose-dependent manner. Treatment with aminoguanidine resulted in an improvement from 15 ± 1%, to 30 ± 2% with 100 µM, and to 37 ± 2% with 300 µM (Fig. 6E). With tenilsetam, we observed an improvement from 34 ± 1% to 48 ± 2% with 100 µM, and to 54 ± 2% with 300 µM (Fig. 6F).

Discussion

At present, the understanding of the molecular mechanisms underlying neurodegeneration in Parkinson's disease and other synucleinopathies is still limited. In particular, the age-dependency of most neurodegenerative disorders is

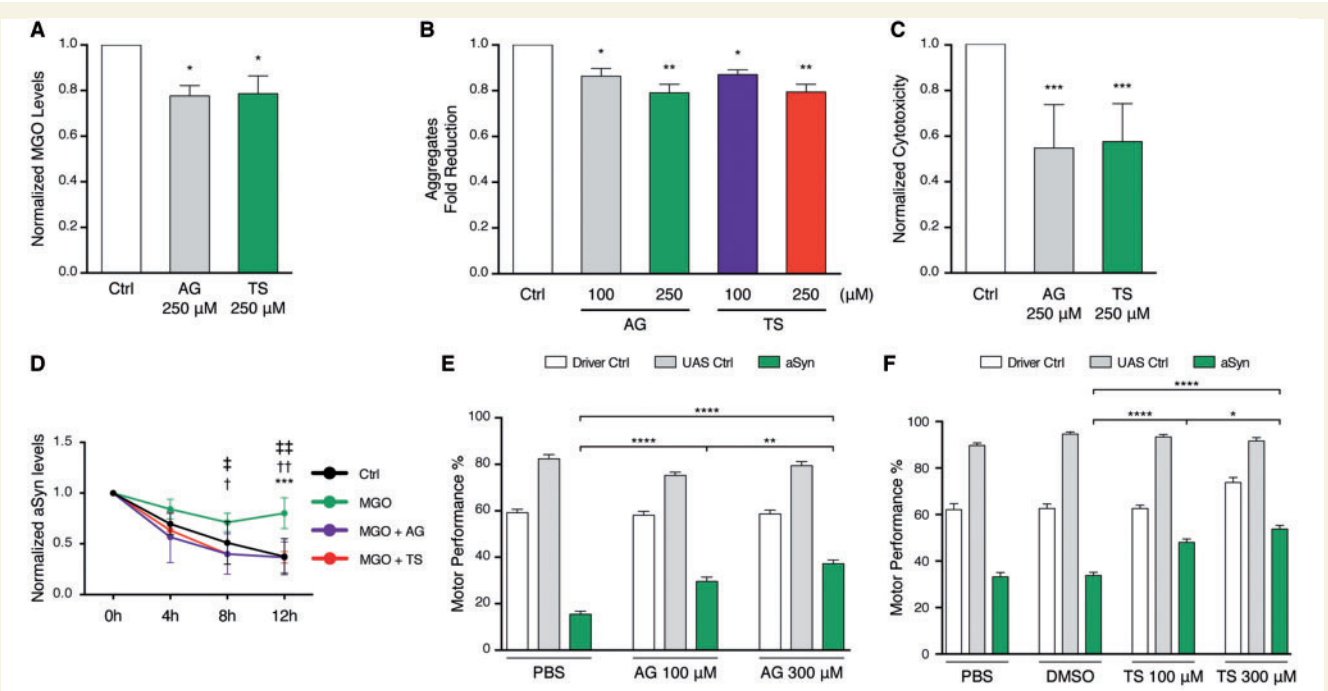

Figure 6 MGO scavengers reduce α-synuclein aggregation and toxicity, increase α-synuclein clearance in mammalian cells, and rescue motor performance in α-synuclein transgenic flies. (**A**) H4 cells co-expressing SynT and Synph 1 were treated with vehicle (Ctrl), aminoguanidine (AG) or tenilsetam (TS) for 16 h. MGO levels were measured by HPLC and normalized to Ctrl. (**B**) H4 cells, as in **A**, were treated with vehicle (Ctrl), aminoguanidine or tenilsetam for 16 h and processed for ICC. Fold-reduction in aggregation is presented ($n = 3$). (**C**) Toxicity of vehicle (Ctrl), aminoguanidine or tenilsetam 22 h-treated cells, as in **A**, measured by lactate dehydrogenase (LDH) release ($n = 3$) and normalized to Ctrl. (**D**) Cells, as in **A** were pretreated with vehicle (Ctrl) or MGO (0.5 mM) for 16 h. Cells were treated with vehicle, MGO, MGO and aminoguanidine, or MGO and tenilsetam for 16 h. Media was replaced and cells were treated again for 12 h, together with cycloheximide for 4, 8 or 12 h. Protein extracts were probed for α-synuclein and β-actin, for normalization. Data for Ctrl and MGO is the same as in Fig. 5B. (**E**) Aminoguanidine and tenilsetam treatment partially rescued the motor performance of α-synuclein flies in dose-dependent manner. Data in **A–C** are average ± SD. Data in **E** and **F** are mean ± SEM. $^{*}P < 0.05$, $^{**}P < 0.01$, $^{***}P < 0.001$, $^{****}P < 0.0001$. For **A**, unpaired two-tailed *t*-test with equal SD; for **B** and **C**, ordinary one-way ANOVA, followed by Dunnett's multiple comparisons test; for **D**, two-way ANOVA, followed by Tukey's multiple comparison test; for **E** and **F**, ordinary one-way ANOVA, followed by Newman-Keuls multiple comparisons test.

intriguing, suggesting common factors may play important roles in both processes. While α-synuclein misfolding and accumulation is a major pathological hallmark in synucleinopathies, α-synuclein mutations occur only in a small fraction of all Parkinson's disease cases. Thus, it is logical to think that non-genetic factors, such as post-translational modifications (PTMs), might modulate the aggregation and toxicity of α-synuclein, as this is common among idiopathic and familial forms of synucleinopathies. Indeed, phosphorylation on S129 and in other sites has been extensively studied and found to modulate α-synuclein aggregation and toxicity in various model systems (Wang *et al.*, 2012; Tenreiro *et al.*, 2014*a*). However, during the normal lifetime of α-synuclein, several other PTMs are likely to occur, thereby modulating its normal behaviour (Oueslati *et al.*, 2010; Gonçalves *et al.*, 2012; Beyer and Ariza, 2013). In this context, we propose that particular PTMs may act as 'second-hits' that induce structural and stability alterations, thereby potentiating α-synuclein aggregation and toxicity.

Although diabetes has been extensively linked to neurodegenerative diseases (Hu *et al.*, 2007; Sun *et al.*, 2012; Crane *et al.*, 2013; Vagelatos and Eslick, 2013; Vicente Miranda *et al.*, 2016*a*), the molecular basis for this connection remains unclear. A known consequence of increased glucose levels is the, unavoidable, age-associated modification of specific amino acid residues in proteins in a process known as glycation, altering protein structure and function (Vicente Miranda and Outeiro, 2010). Importantly, we recently found that glycation potentiates neurodegeneration in models of Huntington's disease (Vicente Miranda *et al.*, 2016*b*), further suggesting an association between hyperglycaemia and neurodegeneration. Strikingly, a recent clinical trial revealed that a drug used to treat diabetes resulted in improvements in both motor and cognitive metrics in Parkinson's disease subjects (Aviles-Olmos *et al.*, 2013). Here, we demonstrated that glycation, a direct consequence of diabetes, might play an important and underappreciated role in Parkinson's disease and other synucleinopathies by modulating α-synuclein biology (Fig. 7).

Exploiting a yeast model of α-synuclein-mediated cellular pathologies, we found that glycation exacerbates α-synuclein toxicity and aggregation, and we then showed this effect was conserved in human cell lines and, importantly, in differentiated patient-derived iPSCs. Interestingly, upon knockdown of α-synuclein in iPSCs, the cytotoxicity of MGO is abolished, confirming that cytotoxicity is associated with the levels of α-synuclein.

Next, we evaluated the effects of glycation in animal models of Parkinson's disease. Remarkably, by promoting α-synuclein glycation through genetic or pharmacological manipulation of MGO levels, we recapitulated several pathological alterations in both α-synuclein transgenic *Drosophila* and mice. Glycation not only reduces the motor performance of α-synuclein expressing flies, but also decreases survival. In α-synuclein expressing mice, MGO injection in the substantia nigra causes an impressive loss of neuronal cells, including TH-positive neurons. Neuritic degeneration extended to the striatum, a region innervated by dopaminergic neurons from the substantia nigra. We also found extensive labelling for aggregated α-synuclein in the substantia nigra pars comapacta and of pS129 α-synuclein, confirming that glycation induces the aggregation of α-synuclein and leads to the accumulation of pathological α-synuclein.

To establish that α-synuclein glycation can indeed affect neuronal function, we used a functional paradigm that enables us to assess the effects of α-synuclein on synaptic transmission. As an experimental paradigm, we used rat hippocampal brain slices (Diogenes *et al.*, 2012). Indeed, we found that glycated α-synuclein impairs hippocampal long-term potentiation.

The concentrations of MGO used in our study are within, or below, the range used in other studies, and resulted in an increase in the levels of intracellular MGO (~36%). Importantly, our findings are strongly supported by genetic manipulations in yeast and flies and, therefore, constitute proof-of-concept that glycation of α-synuclein exacerbates its aggregation and toxicity. Strikingly, we demonstrate that glycated α-synuclein is present in aged human brains. Given the low number of available human brain samples, and the fact that all samples were derived from elderly individuals (>73 years old), we could not establish whether the levels of CEL-glycated α-synuclein were higher in disease versus control brains. Thus, future studies with larger numbers of human brain samples should enable additional confirmation. Nevertheless, using brain tissue from wild-type or human α-synuclein BAC transgenic mice (expressed under the regulation of the human α-synuclein promoter), we observed that the levels of glycated α-synuclein increase with age. These findings strongly support our hypothesis that glycation might be associated with synucleinopathies in an age-dependent manner.

Our *in vitro* studies provide valuable mechanistic insight into the effects glycation has on α-synuclein. We found it increases α-synuclein oligomerization and interferes with the N-terminal structure of the protein, reducing the ability of α-synuclein to bind to lipid membranes. Together, these findings confirm that glycation may perturb the physiological role of α-synuclein on vesicular trafficking (Nemani *et al.*, 2010; Scott *et al.*, 2010).

Given that CEL-glycation occurs specifically in lysine residues, we asked whether it affected α-synuclein ubiquitination and clearance. Our findings confirm our hypothesis, and demonstrate that MGO-treatment, reduced α-synuclein ubiquitination, reduced UPS- (in the α-synuclein aggregation model) and autophagy-lysosome pathway-mediated degradation of α-synuclein, and also the release of α-synuclein from cells. It is possible that the proteasome dysregulation induced by α-synuclein in the conditions tested saturates the system, limiting the ability to detect an additional accumulation of GFPu under glycation conditions. Overall, the failure in these proteostasis components

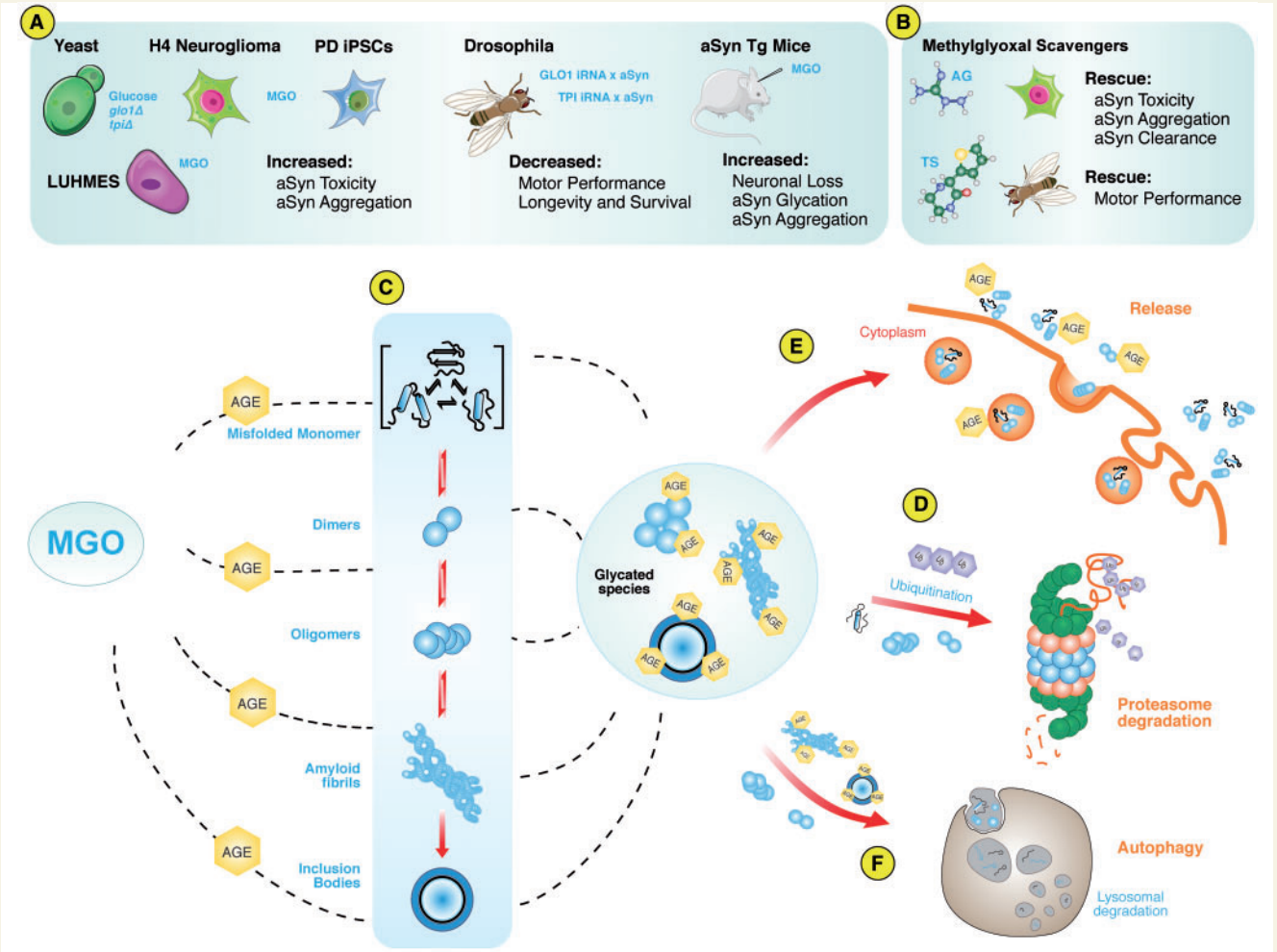

Figure 7 Effects of MGO in models of Parkinson's disease. (**A**) Glycation promotes α-synuclein-mediated toxicity and aggregation in cell models of Parkinson's disease, promotes neuronal loss in mice, and decreases motor performance in *Drosophila*. (**B**) MGO scavengers protect against α-synuclein toxicity and aggregation and improve motor performance in *Drosophila*. (**C**) Mechanistically, glycation induces α-synuclein oligomerization and promotes α-synuclein inclusion formation in cell models of Parkinson's disease. Glycation also decreases α-synuclein clearance by impairing the ubiquitin proteasome system (**D**), the autophagy lysosome pathway (**E**), and the release of α-synuclein (**F**).
AG = aminoguanidine; aSyn = α-synuclein; PD = Parkinson's disease; TS = tenilsetam.

contributes to the accumulation, aggregation and cytotoxicity of α-synuclein.

Finally, we sought to demonstrate the potential value of pharmacological modulation of glycation in models of synucleinopathy. Using anti-glycation agents, we could attenuate or revert the phenotypes observed. Remarkably, we demonstrate that anti-MGO treatment improves motor performance *in vivo* in α-synuclein-expressing flies, and reduces both α-synuclein aggregation and toxicity in cultured cells by restoring α-synuclein clearance.

Generally, glycation is responsible for increasing oxidative stress and inflammation via activation of the receptor for AGE (RAGE) (Bierhaus *et al.*, 2001; Vicente Miranda and Outeiro, 2010). Thus, our findings are in line with previous studies reporting elevated RAGE levels in Parkinson's disease tissue (Dalfo *et al.*, 2005). As RAGE ablation was shown to protect against MPTP/MPP$^+$-induced dopaminergic cell loss (Teismann *et al.*, 2012), we hypothesize that strategies aimed at blocking RAGE might prove valuable in Parkinson's disease.

Our findings further support the hypothesis that hyperglycaemia, which directly correlates with increased levels of MGO, might play an unanticipated role in the molecular basis of Parkinson's disease and other synucleinopathies through the modulation of α-synuclein aggregation, accumulation, and toxicity. This is strongly supported by the fact that diabetes is considered a risk factor for Parkinson's disease (Vicente Miranda *et al.*, 2016*a*). Importantly, a direct genetic association between glycation and Parkinson's disease is already known, although it has not been explored. This link comes from the fact that mutations in DJ-1 (*PARK7*), a protein recently shown to be an anti-MGO enzyme with glyoxalase and deglycase activities (Lee *et al.*, 2012; Mihoub *et al.*, 2015; Richarme *et al.*,

2015), are associated with recessive forms of Parkinson's disease. Importantly, DJ-1 restores the activity of several glycated proteins, including glyceraldehyde-3-phosphate dehydrogenase, aldolase and aspartate aminotransferase. Thus, Parkinson's disease cases associated with DJ-1 mutations might result from excessive protein glycation. Consistently, we already established a physical interaction between DJ-1 and α-synuclein, and showed that human wild-type DJ-1 as well as yeast DJ-1 orthologues, protect against α-synuclein toxicity (Zondler *et al.*, 2014). In our view, this constitutes an important link that is only now beginning to be appreciated, and suggests that the modulation of anti-glycation enzymes, such as DJ-1 or GLO1 (as we demonstrate in the present study), or the direct manipulation of MGO levels using scavengers, constitute novel and attractive strategies for therapeutic intervention in synucleinopathies.

Altogether, our study suggests that glycation may constitute a missing link in our understanding of the molecular pathogenesis of Parkinson's disease and other synucleinopathies, acting as a 'second hit' that increases the risk for disease onset, at least in a significant subset of synucleinopathy patients.

Acknowledgements

LUHMES cells were a kind gift of Dr M. Leist, University of Konstanz, Germany. Methoxy-XO4 was a kind gift from Dr William E. Klunk, University of Pittsburgh, USA. We thank Professor Rui Moreira and Dr Susana Lucas for assistance with MGO purification and measurement, and Diana Macedo for assistance with flow cytometry. We acknowledge the Pathology Department of Hospital de Santa Maria (Lisbon) and to Prof. Matthew Frosch from the Massachusetts Alzheimer's Disease Research Center for kindly providing the human brain samples used in our study. We acknowledge Ana Chegão and Bárbara Gomes for technical assistance during the revision process of the manuscript.

Funding

Authors were supported by: H.V.M. (Fundação para a Ciência e Tecnologia (FCT), Portugal SFRH/BPD/64702/2009 and SFRH/BPD/109347/2015; EU FP7 project MEFOPA), L.M.A.O (FCT - SFRH/BD/23604/2005; CIRM-BMFB joint grant, 315050 AZ0101-31P6855), R.M.O. and T.S. (FCT SFRH/BPD/41416/2007; SFRH/BPD/31209/2006); W.X. (Deutsche Forschungsgemeinschaft, SFB539/A3); C.B. and F.G. (Parkinson's UK and the Medical Research Council, UK). S.E. is supported by Israel Academy of Sciences, Rappaport Family Institute for Research in the Medical Sciences, The Allen and Jewel Prince Center for Neurodegenerative Disorders of the Brain. T.F.O. (EMBO Installation Grant; Marie Curie IRG, Neurofold; DFG Center for Nanoscale Microscopy and Molecular Physiology of the Brain; I.C.M. (FCT SFRH/BPD/74287/2010; Investigador FCT IF/00772/2013). This work was supported by: FCT PTDC/SAU-NEU/105215/2008, PTDC/QUI/73430/2006, PTDC/SAU-ENB/117013/2010, PTDC/NEU-OSD/5644/2014; EU FP7 project MEFOPA; CIRM-BMFB joint grant (315050 AZ0101-31P6855); Max Planck Society; and European Union (NEURASYNC PITNGA-2009-238316).

Supplementary material

Supplementary material is available at *Brain* online.

References

Ahmed MU, Brinkmann Frye E, Degenhardt TP, Thorpe SR, Baynes JW. N-epsilon-(carboxyethyl)lysine, a product of the chemical modification of proteins by methylglyoxal, increases with age in human lens proteins. Biochem J 1997; 324 (Pt 2): 565–70.

Ali YO, Escala W, Ruan K, Zhai RG. Assaying locomotor, learning, and memory deficits in Drosophila models of neurodegeneration. J Vis Exp 2011; 49: e2504.

Anderson JP, Walker DE, Goldstein JM, de Laat R, Banducci K, Caccavello RJ, et al. Phosphorylation of Ser-129 is the dominant pathological modification of alpha-synuclein in familial and sporadic Lewy body disease. J Biol Chem 2006; 281: 29739–52.

Anderson WW, Collingridge GL. The LTP program: a data acquisition program for on-line analysis of long-term potentiation and other synaptic events. J Neurosci Methods 2001; 108: 71–83.

Aviles-Olmos I, Dickson J, Kefalopoulou Z, Djamshidian A, Ell P, Soderlund T, et al. Exenatide and the treatment of patients with Parkinson's disease. J Clin Invest 2013; 123: 2730–6.

Basso E, Antas P, Marijanovic Z, Goncalves S, Tenreiro S, Outeiro TF. PLK2 modulates alpha-synuclein aggregation in yeast and mammalian cells. Mol Neurobiol 2013; 48: 854–62.

Baynes JW, Thorpe SR. Glycoxidation and lipoxidation in atherogenesis. Free Radic Biol Med 2000; 28: 1708–16.

Bence NF, Sampat RM, Kopito RR. Impairment of the ubiquitin-proteasome system by protein aggregation. Science 2001; 292: 1552–5.

Bertoncini CW, Jung YS, Fernandez CO, Hoyer W, Griesinger C, Jovin TM, et al. Release of long-range tertiary interactions potentiates aggregation of natively unstructured alpha-synuclein. Proc Natl Acad Sci USA 2005; 102: 1430–5.

Beyer K, Ariza A. Alpha-synuclein posttranslational modification and alternative splicing as a trigger for neurodegeneration. Mol Neurobiol 2013; 47: 509–24.

Bierhaus A, Fleming T, Stoyanov S, Leffler A, Babes A, Neacsu C, et al. Methylglyoxal modification of Nav1.8 facilitates nociceptive neuron firing and causes hyperalgesia in diabetic neuropathy. Nat Med 2012; 18: 926–33.

Bierhaus A, Schiekofer S, Schwaninger M, Andrassy M, Humpert PM, Chen J, et al. Diabetes-associated sustained activation of the transcription factor nuclear factor-kappaB. Diabetes 2001; 50: 2792–808.

Byers B, Cord B, Nguyen HN, Schule B, Fenno L, Lee PC, et al. SNCA triplication Parkinson's patient's iPSC-derived DA neurons accumulate alpha-synuclein and are susceptible to oxidative stress. PloS One 2011; 6: e26159.

Castellani R, Smith MA, Richey PL, Perry G. Glycoxidation and oxidative stress in Parkinson disease and diffuse Lewy body disease. Brain Res 1996; 737: 195–200.

Chang TJ, Tseng HC, Liu MW, Chang YC, Hsieh ML, Chuang LM. Glucagon-like peptide-1 prevents methylglyoxal-induced apoptosis of beta cells through improving mitochondrial function and suppressing prolonged AMPK activation. Sci Rep 2016; 6: 23403.

Chen TS, Richie JP Jr, Lang CA. The effect of aging on glutathione and cysteine levels in different regions of the mouse brain. Proc Soc Exp Biol Med 1989; 190: 399–402.

Crane PK, Walker R, Hubbard RA, Li G, Nathan DM, Zheng H, et al. Glucose levels and risk of dementia. N Engl J Med 2013; 369: 540–8.

Dalfo E, Portero-Otin M, Ayala V, Martinez A, Pamplona R, Ferrer I. Evidence of oxidative stress in the neocortex in incidental Lewy body disease. J Neuropathol Exp Neurol 2005; 64: 816–30.

Delaglio F, Grzesiek S, Vuister GW, Zhu G, Pfeifer J, Bax A. NMRPipe: a multidimensional spectral processing system based on UNIX pipes. J Biomol NMR 1995; 6: 277–93.

Diogenes MJ, Costenla AR, Lopes LV, Jeronimo-Santos A, Sousa VC, Fontinha BM, et al. Enhancement of LTP in aged rats is dependent on endogenous BDNF. Neuropsychopharmacology 2011; 36: 1823–36.

Diogenes MJ, Dias RB, Rombo DM, Vicente Miranda H, Maiolino F, Guerreiro P, et al. Extracellular alpha-synuclein oligomers modulate synaptic transmission and impair LTP via NMDA-receptor activation. J Neurosci 2012; 32: 11750–62.

Ebrahimi-Fakhari D, Wahlster L, McLean PJ. Protein degradation pathways in Parkinson's disease: curse or blessing. Acta Neuropathol 2012; 124: 153–72.

Faustino AF, Carvalho FA, Martins IC, Castanho MA, Mohana-Borges R, Almeida FC, et al. Dengue virus capsid protein interacts specifically with very low-density lipoproteins. Nanomedicine 2014; 10: 247–55.

Feany MB, Bender WW. A Drosophila model of Parkinson's disease. Nature 2000; 404: 394–8.

Fredholm BB, Dunwiddie TV, Bergman B, Lindstrom K. Levels of adenosine and adenine nucleotides in slices of rat hippocampus. Brain Res 1984; 295: 127–36.

Frye EB, Degenhardt TP, Thorpe SR, Baynes JW. Role of the Maillard reaction in aging of tissue proteins. Advanced glycation end product-dependent increase in imidazolium cross-links in human lens proteins. J Biol Chem 1998; 273: 18714–19.

Gomes RA, Sousa Silva M, Vicente Miranda H, Ferreira AE, Cordeiro CA, Freire AP. Protein glycation in Saccharomyces cerevisiae. Argpyrimidine formation and methylglyoxal catabolism. FEBS J 2005; 272: 4521–31.

Gonçalves S, Vicente Miranda H, Outeiro TF. Novel molecular therapeutics in Parkinson's disease. In: Whitehouse D, Rapley R, editors. Molecular and cellular therapeutics. Chichester, UK: John Wiley & Sons, Ltd; 2012. p. 245–65.

Guerreiro PS, Huang Y, Gysbers A, Cheng D, Gai WP, Outeiro TF, et al. LRRK2 interactions with alpha-synuclein in Parkinson's disease brains and in cell models. J Mol Med 2013; 91: 513–22.

Guix FX, Ill-Raga G, Bravo R, Nakaya T, de Fabritiis G, Coma M, et al. Amyloid-dependent triosephosphate isomerase nitrotyrosination induces glycation and tau fibrillation. Brain 2009; 132 (Pt 5): 1335–45.

Hansen F, Battu CE, Dutra MF, Galland F, Lirio F, Broetto N, et al. Methylglyoxal and carboxyethyllysine reduce glutamate uptake and S100B secretion in the hippocampus independently of RAGE activation. Amino Acids 2016; 48: 375–85.

Hu G, Jousilahti P, Bidel S, Antikainen R, Tuomilehto J. Type 2 diabetes and the risk of Parkinson's disease. Diabetes care 2007; 30: 842–7.

Jo E, McLaurin J, Yip CM, St George-Hyslop P, Fraser PE. Alpha-synuclein membrane interactions and lipid specificity. J Biol Chem 2000; 275: 34328–34.

Karpinar DP, Balija MB, Kugler S, Opazo F, Rezaei-Ghaleh N, Wender N, et al. Pre-fibrillar alpha-synuclein variants with impaired beta-structure increase neurotoxicity in Parkinson's disease models. EMBO J 2009; 28: 3256–68.

Klionsky DJ, Abdelmohsen K, Abe A, Abedin MJ, Abeliovich H, Acevedo Arozena A, et al. Guidelines for the use and interpretation of assays for monitoring autophagy (3rd edition). Autophagy 2016; 12: 1–222.

Klucken J, Poehler AM, Ebrahimi-Fakhari D, Schneider J, Nuber S, Rockenstein E, et al. Alpha-synuclein aggregation involves a bafilomycin A 1-sensitive autophagy pathway. Autophagy 2012; 8: 754–66.

Klunk WE, Bacskai BJ, Mathis CA, Kajdasz ST, McLellan ME, Frosch MP, et al. Imaging Abeta plaques in living transgenic mice with multiphoton microscopy and methoxy-X04, a systemically administered Congo red derivative. J Neuropathol Exp Neurol 2002; 61: 797–805.

Kuhla B, Boeck K, Luth HJ, Schmidt A, Weigle B, Schmitz M, et al. Age-dependent changes of glyoxalase I expression in human brain. Neurobiol Aging 2006; 27: 815–22.

Lashuel HA, Hartley D, Petre BM, Walz T, Lansbury PT Jr. Neurodegenerative disease: amyloid pores from pathogenic mutations. Nature 2002a; 418: 291.

Lashuel HA, Petre BM, Wall J, Simon M, Nowak RJ, Walz T, et al. Alpha-synuclein, especially the Parkinson's disease-associated mutants, forms pore-like annular and tubular protofibrils. J Mol Biol 2002b; 322: 1089–102.

Lazaro DF, Rodrigues EF, Langohr R, Shahpasandzadeh H, Ribeiro T, Guerreiro P, et al. Systematic comparison of the effects of alpha-synuclein mutations on its oligomerization and aggregation. PLoS Genet 2014; 10: e1004741.

Lee D, Park CW, Paik SR, Choi KY. The modification of alpha-synuclein by dicarbonyl compounds inhibits its fibril-forming process. Biochim Biophys Acta 2009; 1794: 421–30.

Lee JY, Song J, Kwon K, Jang S, Kim C, Baek K, et al. Human DJ-1 and its homologs are novel glyoxalases. Hum Mol Genet 2012; 21: 3215–25.

Lyles GA, Chalmers J. The metabolism of aminoacetone to methylglyoxal by semicarbazide-sensitive amine oxidase in human umbilical artery. Biochem Pharmacol 1992; 43: 1409–14.

Macedo D, Tavares L, McDougall GJ, Vicente Miranda H, Stewart D, Ferreira RB, et al. (Poly)phenols protect from alpha-synuclein toxicity by reducing oxidative stress and promoting autophagy. Hum Mol Genet 2015; 24: 1717–32.

Mak SK, Huang YA, Iranmanesh S, Vangipuram M, Sundararajan R, Nguyen L, et al. Small molecules greatly improve conversion of human-induced pluripotent stem cells to the neuronal lineage. Stem Cells Int 2012; 2012: 140427.

Marques O, Outeiro TF. Alpha-synuclein: from secretion to dysfunction and death. Cell Death Dis 2012; 3: e350.

Martins IC, Kuperstein I, Wilkinson H, Maes E, Vanbrabant M, Jonckheere W, et al. Lipids revert inert Abeta amyloid fibrils to neurotoxic protofibrils that affect learning in mice. EMBO J 2008; 27: 224–33.

McLean PJ, Kawamata H, Hyman BT. Alpha-synuclein-enhanced green fluorescent protein fusion proteins form proteasome sensitive inclusions in primary neurons. Neuroscience 2001; 104: 901–12.

Mihoub M, Abdallah J, Gontero B, Dairou J, Richarme G. The DJ-1 superfamily member Hsp31 repairs proteins from glycation by methylglyoxal and glyoxal. Biochem Biophys Res Commun 2015; 463: 1305–10.

Munch G, Luth HJ, Wong A, Arendt T, Hirsch E, Ravid R, et al. Crosslinking of alpha-synuclein by advanced glycation endproducts–an early pathophysiological step in Lewy body formation?. J Chem Neuroanat 2000; 20: 253–7.

Naiki H, Higuchi K, Hosokawa M, Takeda T. Fluorometric determination of amyloid fibrils *in vitro* using the fluorescent dye, thioflavin T1. Anal Biochem 1989; 177: 244–9.

Naiki H, Higuchi K, Matsushima K, Shimada A, Chen WH, Hosokawa M, et al. Fluorometric examination of tissue amyloid

fibrils in murine senile amyloidosis: use of the fluorescent indicator, thioflavine T. Lab Invest 1990; 62: 768–73.
Nass N, Bromme HJ, Hartig R, Korkmaz S, Sel S, Hirche F, et al. Differential response to alpha-oxoaldehydes in tamoxifen resistant MCF-7 breast cancer cells. PloS One 2014; 9: e101473.
Nemani VM, Lu W, Berge V, Nakamura K, Onoa B, Lee MK, et al. Increased expression of alpha-synuclein reduces neurotransmitter release by inhibiting synaptic vesicle reclustering after endocytosis. Neuron 2010; 65: 66–79.
Nonaka T, Iwatsubo T, Hasegawa M. Ubiquitination of alpha-synuclein. Biochemistry 2005; 44: 361–8.
Oliveira LM, Falomir-Lockhart LJ, Botelho MG, Lin KH, Wales P, Koch JC, et al. Elevated alpha-synuclein caused by SNCA gene triplication impairs neuronal differentiation and maturation in Parkinson's patient-derived induced pluripotent stem cells. Cell Death Dis 2015; 6: e1994.
Oliveira LM, Gomes RA, Yang D, Dennison SR, Familia C, Lages A, et al. Insights into the molecular mechanism of protein native-like aggregation upon glycation. Biochim Biophys Acta 2013; 1834: 1010–22.
Oliveira LM, Lages A, Gomes RA, Neves H, Familia C, Coelho AV, et al. Insulin glycation by methylglyoxal results in native-like aggregation and inhibition of fibril formation. BMC Biochem 2011; 12: 41.
Orosz F, Olah J, Ovadi J. Triosephosphate isomerase deficiency: new insights into an enigmatic disease. Biochim Biophys Acta 2009; 1792: 1168–74.
Oueslati A, Fournier M, Lashuel HA. Role of post-translational modifications in modulating the structure, function and toxicity of alpha-synuclein: implications for Parkinson's disease pathogenesis and therapies. Prog Brain Res 2010; 183: 115–45.
Outeiro TF, Lindquist S. Yeast cells provide insight into alpha-synuclein biology and pathobiology. Science 2003; 302: 1772–5.
Padmaraju V, Bhaskar JJ, Prasada Rao UJ, Salimath PV, Rao KS. Role of advanced glycation on aggregation and DNA binding properties of alpha-synuclein. J Alzheimers Dis 2011; 24 (Suppl 2): 211–21.
Pearce RK, Owen A, Daniel S, Jenner P, Marsden CD. Alterations in the distribution of glutathione in the substantia nigra in Parkinson's disease. J Neural Transm 1997; 104: 661–77.
Reichard GA Jr, Skutches CL, Hoeldtke RD, Owen OE. Acetone metabolism in humans during diabetic ketoacidosis. Diabetes 1986; 35: 668–74.
Richard JP. Mechanism for the formation of methylglyoxal from triosephosphates. Biochem Soc Trans 1993; 21: 549–53.
Richarme G, Mihoub M, Dairou J, Bui LC, Leger T, Lamouri A. Parkinsonism-associated protein DJ-1/Park7 is a major protein deglycase that repairs methylglyoxal- and glyoxal-glycated cysteine, arginine, and lysine residues. J Biol Chem 2015; 290: 1885–97.
Rockenstein E, Mallory M, Hashimoto M, Song D, Shults CW, Lang I, et al. Differential neuropathological alterations in transgenic mice expressing alpha-synuclein from the platelet-derived growth factor and Thy-1 promoters. J Neurosci Res 2002; 68: 568–78.
Schiff SJ, Somjen GG. The effects of temperature on synaptic transmission in hippocampal tissue slices. Brain Res 1985; 345: 279–84.
Scholz D, Poltl D, Genewsky A, Weng M, Waldmann T, Schildknecht S, et al. Rapid, complete and large-scale generation of post-mitotic neurons from the human LUHMES cell line. J Neurochem 2011; 119: 957–71.
Scott DA, Tabarean I, Tang Y, Cartier A, Masliah E, Roy S. A pathologic cascade leading to synaptic dysfunction in alpha-synuclein-induced neurodegeneration. J Neurosci 2010; 30: 8083–95.
Spillantini MG, Crowther RA, Jakes R, Hasegawa M, Goedert M. Alpha-synuclein in filamentous inclusions of Lewy bodies from Parkinson's disease and dementia with lewy bodies. Proc Natl Acad Sci USA 1998; 95: 6469–73.
Strohalm M, Kavan D, Novak P, Volny M, Havlicek V. mMass 3: a cross-platform software environment for precise analysis of mass spectrometric data. Anal Chem 2010; 82: 4648–51.
Sun Y, Chang YH, Chen HF, Su YH, Su HF, Li CY. Risk of Parkinson disease onset in patients with diabetes: a 9-year population-based cohort study with age and sex stratifications. Diabetes Care 2012; 35: 1047–9.
Szego EM, Gerhardt E, Kermer P, Schulz JB. A30P alpha-synuclein impairs dopaminergic fiber regeneration and interacts with L-DOPA replacement in MPTP-treated mice. Neurobiol Dis 2012; 45: 591–600.
Szego EM, Outeiro TF, Kermer P, Schulz JB. Impairment of the septal cholinergic neurons in MPTP-treated A30P alpha-synuclein mice. Neurobiol Aging 2013; 34: 589–601.
Teismann P, Sathe K, Bierhaus A, Leng L, Martin HL, Bucala R, et al. Receptor for advanced glycation endproducts (RAGE) deficiency protects against MPTP toxicity. Neurobiol Aging 2012; 33: 2478–90.
Tenreiro S, Eckermann K, Outeiro TF. Protein phosphorylation in neurodegeneration: friend or foe?. Front Mol Neurosci 2014a; 7: 42.
Tenreiro S, Outeiro TF. Simple is good: yeast models of neurodegeneration. FEMS Yeast Res 2010; 10: 970–9.
Tenreiro S, Reimao-Pinto MM, Antas P, Rino J, Wawrzycka D, Macedo D, et al. Phosphorylation modulates clearance of alpha-synuclein inclusions in a yeast model of Parkinson's disease. PLoS Genet 2014b; 10: e1004302.
Thornalley PJ, Langborg A, Minhas HS. Formation of glyoxal, methylglyoxal and 3-deoxyglucosone in the glycation of proteins by glucose. Biochem J 1999; 344 (Pt 1): 109–16.
Tiscornia G, Singer O, Verma IM. Production and purification of lentiviral vectors. Nat Protoc 2006; 1: 241–5.
Vagelatos NT, Eslick GD. Type 2 diabetes as a risk factor for Alzheimer's disease: the confounders, interactions, and neuropathology associated with this relationship. Epidemiol Rev 2013; 35: 152–60.
Vander Jagt DL, Robinson B, Taylor KK, Hunsaker LA. Reduction of trioses by NADPH-dependent aldo-keto reductases. Aldose reductase, methylglyoxal, and diabetic complications. J Biol Chem 1992; 267: 4364–9.
Vicente Miranda H, El-Agnaf OM, Outeiro TF. Glycation in Parkinson's disease and Alzheimer's disease. Mov Disord 2016a; 31: 782–90.
Vicente Miranda H, Gomes MA, Branco-Santos J, Breda C, Lazaro DF, Lopes LV, et al. Glycation potentiates neurodegeneration in models of Huntington's disease. Sci Rep 2016b; 6: 36798.
Vicente Miranda H, Outeiro TF. The sour side of neurodegenerative disorders: the effects of protein glycation. J Pathol 2010; 221: 13–25.
Vicente Miranda H, Xiang W, de Oliveira RM, Simoes T, Pimentel J, Klucken J, et al. Heat-mediated enrichment of alpha-synuclein from cells and tissue for assessing post-translational modifications. J Neurochem 2013; 126: 673–84.
Wales P, Pinho R, Lazaro DF, Outeiro TF. Limelight on alpha-synuclein: pathological and mechanistic implications in neurodegeneration. J Parkinsons Dis 2013; 3: 415–59.
Wang Y, Shi M, Chung KA, Zabetian CP, Leverenz JB, Berg D, et al. Phosphorylated alpha-synuclein in Parkinson's disease. Sci Transl Med 2012; 4: 121ra20.
Webster J, Urban C, Berbaum K, Loske C, Alpar A, Gartner U, et al. The carbonyl scavengers aminoguanidine and tenilsetam protect against the neurotoxic effects of methylglyoxal. Neurotox Res 2005; 7: 95–101.
Willingham S, Outeiro TF, DeVit MJ, Lindquist SL, Muchowski PJ. Yeast genes that enhance the toxicity of a mutant huntingtin fragment or alpha-synuclein. Science 2003; 302: 1769–72.
Yao D, Brownlee M. Hyperglycemia-induced reactive oxygen species increase expression of the receptor for advanced glycation end products (RAGE) and RAGE ligands. Diabetes 2010; 59: 249–55.
Zondler L, Miller-Fleming L, Repici M, Goncalves S, Tenreiro S, Rosado-Ramos R, et al. DJ-1 interactions with alpha-synuclein attenuate aggregation and cellular toxicity in models of Parkinson's disease. Cell Death Dis 2014; 5: e1350.